Petrographic characterization of historic mortar as a tool in archaeologic study: Examples from two medieval castles of Aosta Valley, Northwestern Italy

Published version:

DOI:10.1016/j.jasrep.2022.103719

E. Milanesio, E. Storta, F. Gambino, L. Appolonia, A. Borghi, A. Glarey *(2022)*

Petrographic characterization of historic mortar as a tool in archaeologic

study: Examples from two medieval castles of Aosta Valley,

Northwestern Italy

Journal of Archaeological Science: Reports, **46, 103719**

Petrographic characterization of historic mortar as a tool in archaeologic study: examples from two medieval castles of Aosta Valley, Northwestern Italy

Abstract

In the present work is reported the study of historical mortars sampled in the two medieval castles of Châtel Argent and Quart (Aosta Valley, NW Italy), which in recent years are subject to restoration projects.

All the samples were subjected to a petrographic analyses with an optical microscope, in order to recognize and compare the minerals constituting the main aggregates with the geological formations surrounding the areas where the castles stand.

Four mortar samples were analyzed for each castle with the scanning electron microscope (SEM-EDS system). This procedure allows us to know the composition of the binder (not distinguishable on the basis of a petrographic analyses under an optical microscope), to calculate indices related to the composition of the binder, to analyze the composition of the main minerals present in the aggregate.

Then, compositional X-ray maps were performed, in order to investigate the relative abundances of the different elements and calculate other important information of the mortars such as the hydraulic index, the porosity distribution and the abundance of aggregate with respect to the binder.

The analytical protocol allowed us to define not only the characteristics of the individual mortars, but also to detect the area of provenance of the raw materials used for their realization, guiding the choice of the best materials for future restoration operations.

Key word: historic mortar, hydraulic index, binder, SEM – EDS facility, X-ray maps, provenance.

1. Introduction

Mortars, since ancient times, are an artificial and man-made product made up of natural materials usually obtained by the firing of carbonate or gypsum. By this process, the binder forms and, only after the mixing with aggregate and water, it hardens becoming a mortar (Pecchioni et al., 2018).

The use of mortars seems to have origin in prehistoric times. The discovery probably occurred as the result of an accidental event: the firing of a carbonate rock. It would have been reduced to a powder by heating (calcination process) then extinguished with water and hardened in the air (Schiele and Berens, 1976).

In ancient times, people used different types of both binders and mortars for different purposes; these materials were known in Asia, Mesopotamia, the Near East and Egypt (Elsen, 2006). The

Minoan civilization handed down to the Greeks the art of lime production that was in turn transmitted to the Etruscans (Moropoulou et al., 2000). The Romans increased the Greeks knowledge of mortars and began to spread out the use of these materials, improving their physical and chemical characteristics (Lezzerini et al., 2017, Miriello et al., 2010). Thanks to the Romans, their writings and the study of the several Roman buildings still in good conditions, the advanced techniques of mortar production are nowadays known.

However, during history and especially in the Middle Ages, the techniques of building constructions changed considerably. Mortars with a totally different composition from the Roman parameters were found especially in Italy, France and England (Rampazzi et al., 2016). In the medieval period, moreover, it seems that organic additives such as animal fat, linseed oil, albumen, blood and natural resins were used (Rapp, 2009).

Currently, according to NORMA UNI 10924, 2001, mortars are defined as a mixture of binders (organic or inorganic), aggregates (mainly of fine grain size) and water, to which it is possible to add one or more organic or inorganic additives, in order to improve and/or control the laying conditions of the mix, their physical characteristics (e.g., porosity, water permeability) and mechanical characteristics as resistance, deformability, adherence to surfaces, etc.

The presence and the abundance of MgO compared to CaO is an important aspect to be analyzed. In fact, magnesian mortars tend to have more shrinkage porosity due to the drying process that causes stress around the smallest pores and defines the cracking in the mortar (Sherer, 1990). Magnesian mortars are also characterized by very low mechanical strength also because of internal stresses and shrinkage (Arizzi and Cultrone, 2012).

The petrographic study of mortars, in particular of aggregates, when compared with regional geology, allows us to obtain important information on the source areas of the raw materials with which they were made. Mortars characterization has been performed by combining macroscopic observations, minero-petrographic and micro-chemical techniques as shown in several works focused on this topic (Cantù et al., 2015; Lezzerini et al., 2018; Pecchioni et al., 2018; Riccardi et al., 2007).

In this article a petrographic approach was adopted involving optical microscopy (OM) and Electron Microscopy with X-ray analysis (SEM-EDS system) to characterize the mortars of two medieval castles used as military and lookout fortresses and therefore placed in tactical and inaccessible mountainous positions located in the Aosta Valley (NW Italy).

2. Historic framework

2.1 *Châtel-Argent Castle*

The Castle of Châtel Argent, also called Castle of Villeneuve, is located on a rocky terrace at the valley outlet, to the orographic right of the Dora Baltea River, in the territory of the village of Villeneuve (**Figure 1a**). The surviving structure dates back to the 13th century, but there is evidence that the spur from the important strategic position on which it stands has been used since ancient times, especially by the Romans (De Gattis and Cortellazzo, 2008). Châtel-Argent represents the classic fortified complex, which probably over the centuries was increasingly expanded in the territory and enriched with works, defensive or not. To date, in the Châtel-Argent complex, the remains of a building and a cistern dating back to the 13th century and a better-preserved portion consisting of a cylindrical tower 16 m high and with a diameter of 9.5 m are recognizable.

2.2 *Quart Castle*

The Quart Castle is located in a lookout position, on a steep promontory at the beginning on the left bank of the Dora Baltea River, in the Aosta Valley (**Figure 1b**). The castle consists of several buildings placed on different levels that were built in different eras and it seems that the first works began between the 11th and 12th centuries (Appolonia et al., 2006). The functions of this fortress diversified over time also by means of the different families who took charge of it over the centuries. Since its primitive phase the castle, used for defensive purposes, as a residence and territorial/organizational reference point for an agro-pastoral activity, was always a power center of several noble families. Only at the beginning of the 19th century the castle was sold to the municipality of Quart and in the mid-20th century it became the property of the regional administration of the Aosta Valley (Appolonia et al., 2006).

Figure 1: Châtel Argent Castle (a); Quart Castle (b).

3. Geological setting of Aosta Valley

The two castles of Châtel Argent and Quart are located respectively upstream and downstream of Aosta town, the regional capital of Aosta Valley. The city of Aosta is placed in the middle of the Alpine orogenic chain and is geologically located within the Combin Zone (De Giusti et al., 2004; **Figure 2**) which represents the metamorphic product of the Piemonte-Liguria Ocean originally interposed in the Mesozoic age between the Paleo-European and Insubric continental margins (e.g., Dal Piaz, 1999; Beltrando et al., 2010). The Piemonte Zone includes two main tectonic units, called Zermatt-

Saas Zone (lower) and Combin Zone (upper). The Zermatt-Saas Zone is dominated by ophiolites deriving from a basic and ultra-basic protolite. The metamorphic evolution is characterized by a first event developed under eclogitic facies of the Eocene age, followed by a retrograde event in greenschist facies conditions (Ernst and Dal Piaz, 1978; Beltrando et al., 2010). The upper Piemonte nappe (Combin Zone) consists mainly of Mesozoic metasediments (calcschist and impure marble) interbedded with tabular levels of metabasites (prasinite) and slices of serpentinite and minor meta-gabbro. The Combin Zone shows metamorphic relict in blueschist facies conditions, strongly retrogressed to greenschist facies in the Eocene-Oligocene age (Dal Piaz 1999; De Giusti et al., 2004). Near the city of Aosta, other important geological units of the Alpine chain also outcrop. They consist of different varieties of continental crust rocks such as the klippe of Monte Emilius (equilibrated in eclogitic facies), the nappes of Dent Blanche and Mont Mary (metamorphosed in greenschist facies) belonging to the Austroalpine domain (Dal Piaz, 1999). The Dent Blanche nappe consists of a lower unit (Arolla Gneiss) of prevalent orthogneiss metamorphosed under greeenschist facies conditions and an upper unit (Valpelline Serie) formed by high grade metapelite and metabasite of pre-Alpine age. In the easternmost portion of the Aosta Valley the Sesia Lanzo Zone crops out, a unit of continental crust metamorphosed into eclogitic facies in the Alpine age and partially retrocessed to greenschist facies (Dal Piaz et al., 1972). The Pennidic Domain consists of the internal crystalline massifs of Gran Paradiso (GP) and Monte Rosa (MR) Massifs, both metamorphosed in eclogitic conditions, in addition to the different units of the Gran St. Bernard (GSB) Nappe, metamorphosed in blueschist facies conditions, and the Houillère Zone equilibrated in greenschist facies. These units are mainly made up of mono- and poly-metamorphic micaschist and ortho-derivate with minor metabasite and marble, which represent the metamorphic product of original Mesozoic covering sequences (e.g., De Giusti et al., 2004; Malusà et al., 2005). Finally, in the outermost position of the Pennidic domain, the Sion – Courmayeur Zone crops out (Elter and Elter, 1965), consisting of two main geological units: the Roignais-Versoyen Unit and the Brèches de Tarentaise Unit. The first is composed of oceanic metasediments, metabasites and serpentinized lherzolites of Mesozoic age. The latter consists of carbonate and pelitic metasediments with bodies of polygenic breccias, and are interpreted as a high-pressure metamorphosed flysch deposited in the oceanic trench during Alpine convergence (Loprieno et al., 2011).

The Aosta Valley geology is completed by the Mont Blanc massif, a crustal unit of Helvetic Domain, with the related covers from the Meso-Cenozoic age.

As regards the lithologies on which the castles of Châtel-Argent and Quart insist, we refer to the 1: 50,000 cartography of each area (De Giusti et al., 2004; Polino et al., 2015, with Ref.). The Châtel Argent Castle stands on a marble ridge, interlayed within a body of calcschists belonging to the basal portions of the Combin Zone. The Quart Castle is located in an area where the lower unit of Mont Mary out crops, which is part of the upper nappes of the Austroalpine Domain. The unit in question is described as consisting of schists with quartz, biotite, garnet ± muscovite. In the area also occurs a level of carbonate cover, consisting of meta-dolostone (Roisan Zone), which detach two sub-units of the Mont Mary with Arolla unit.

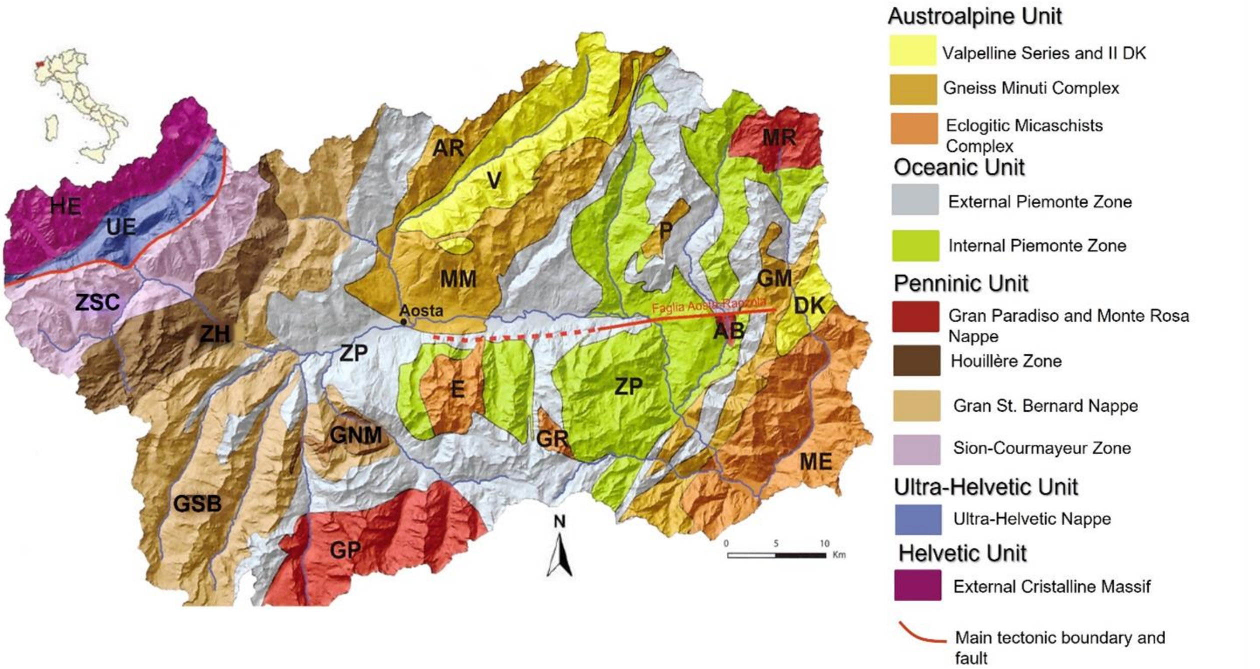

Figure 2: Geological-structural map of Aosta Valley. AB: Arcesaz-Brusson; AR: Arolla Series; DK: Dioritic-Kinzigitic Zone; E: Emilius; GM: Gneiss Minuti Complex; GNM: Gran Nomenon; GR: Glacier Refray; GP: Gran Paradiso; GSB: Gran St. Bernard Nappe; HE: Helvetic; ME: Mount Emilius; MR: Monte Rosa; MM: Mont Mary; P: Pillonet; UE: Ultra Helvetic; V: Valpelline; ZH: Zone Houillère; ZP: Piemonte Zone; ZSC: Sion-Courmayeur Zone (Modified by Martinotti et al., 2011).

4. Materials and methods

The thirty-six samples were analyzed for this work. Twenty of these were sampled in the Quart Castle, while sixteen were sampled at the Châtel Argent Castle. **Figure 3a** and **Figure 3b** shows the sampling site, while **Table 1** the intended use of the samples.

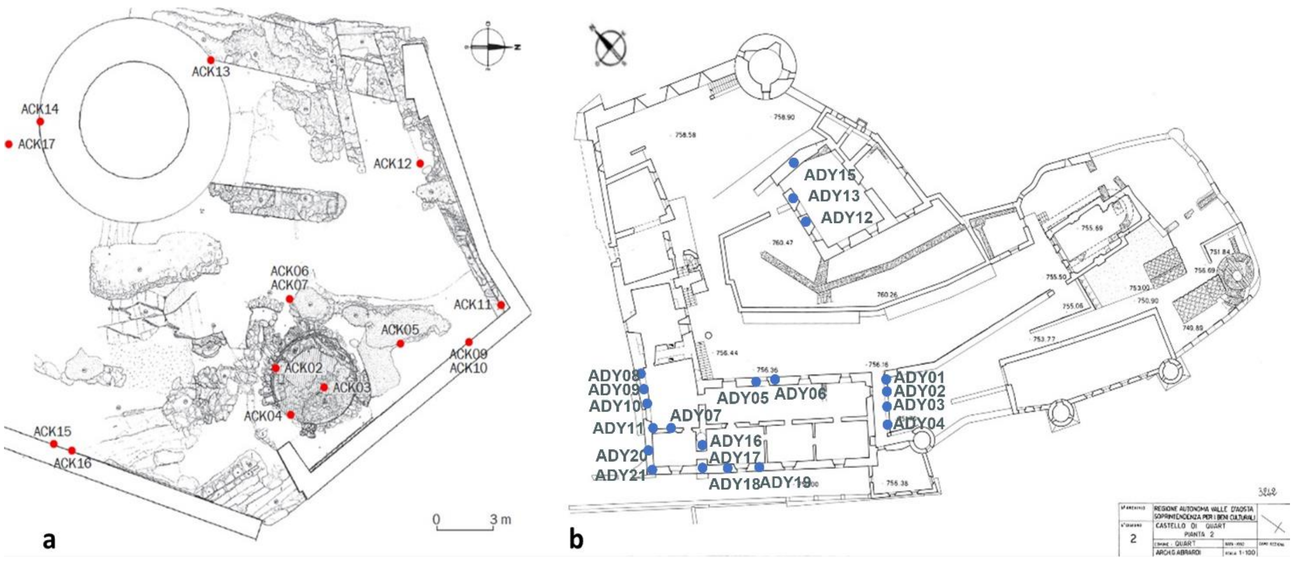

Figure 3: Planimetry of Châtel Argent Castle; the acronyms show the sampling points (a) (modified by Appolonia et al., 2010) and planimetry of Quart Castle (b); the acronyms show the sampling points (modified by Appolonia et al., 2006).

Châtel Argent Castle		Quart Castle	
Sample	*Type of survey*	*Sample*	*Type of survey*
ACK01	Lime fragment with coal	ADY01	Plaster upper balcony (150 cm, date about 1400-1500)
ACK02	Lime inside the kiln	ADY02	Plaster balcony in front of access stairs (135 cm)
ACK03	Lime inside the kiln	ADY03	Upper balcony (260 cm)
ACK04	Lime inside the kiln	ADY04	Plastering upper balcony, 1st floor scaffold
ACK05	Lime cooling zone	ADY05	Plaster over door, external main hall (338 cm)
ACK06	Lime cooling zone	ADY06	Inside window, outside main hall (150 cm)
ACK07	Lime cooling zone	ADY07	Plaster left arch of Savoia building
ACK08	Sample of Bardiglio Marble	ADY08	Plaster room 26 (150 cm)
ACK09	Smooth surface mortar	ADY09	Plaster pre-Montiglio
ACK10	North wall below ACK09	ADY10	Plaster under window
ACK11	Smooth surface mortar	ADY11	Pink plaster
ACK12	West wall	ADY12	Donjon Plaster
ACK13	Tower, west side	ADY13	Donjon plaster, burned
ACK14	Tower, smooth surface mortar	ADY15	Donjon plaster (1556)
ACK15	Smooth surface mortar	ADY16	Mortar Pre-Savoia passage, room 27 and 28
ACK16	Just below ACK15	ADY17	Plaster, Savoia room 28
ACK17	Wall near tank entrance	ADY18	Ancient mortar, arcade room 28
		ADY19	Window draft, outside room 28
		ADY20	Stillness near the ceiling, room 27
		ADY21	Tough mortar, room 27

Table 1: Sample and type of survey respectively for Châtel Argent Castle (on the left) and Quart Castle (on the right).

All the samples were subjected to a petrographic analysis with an optical microscope, through which the main minerals making up the aggregate were recognized. It was performed using a Leitz Laborlux 11 Pol microscope with a 10x Leitz wetzlar periplan eyepiece. In addition to the petrographic analyses, four mortar samples were analyzed for each castle using a scanning electron microscope (SEM-EDS system) and a X-ray powder diffractometer. This procedure allowed to: 1) - know the composition of the binder (which is not distinguishable on the basis of an optical microscope analysis); 2) - analyze the composition of the main minerals present in the samples; 3) - identify the composition and the petrographic nature of some elements of the aggregate that are not easily recognizable under the optical microscope. For 2 samples (ACK17 sample from Châtel Argent Castle and ADY17 sample from Quart Castle) a set of compositional maps were performed, in order to analyze the relative abundances of the different elements and calculate other important information of the mortars, such as porosity, the abundance of aggregate with respect to the binder and the distribution of the aggregate within the binder.

4.1 COMPOSITION OF THE MINERALOGICAL PHASES

The data concerning the chemical composition of the mineralogical phases of the mortars were analyzed with a JEOL IT300 LV SEM equipped with a X-Act3 SDD-EDX detector. The operating conditions were potential difference = 15Kv, beam current = 800pA, working distance = 10mm, counting times = 25s. Cobalt was used as a reference standard and the analyzed sections were previously polished and metallized with graphite. The mineral analyses were acquired using the INCA 300 operating system of Oxford Instruments and were recalculated using the MINSORT software (Petrakakis and Dietrich, 1985).

The values reported in the text of the various elements making up the mineralogical phases are to be considered expressed in atoms per unit of formula (a.p.u.f.). The acronyms of the minerals used in the text are taken from Whitney and Evans (2010).

In order to confirm the obtained classification, the mineralogical composition of the binder was checked by X-ray powder diffraction (XRPD) analyses. XRPD evaluation was conducted on representative samples of both Castles. XRPD patterns were collected by using an Analytical Rigaku "Miniflex II" equipped with an D/teX Ultra: silicon strip detector powder diffractometer using Cu Kα radiation generated at 30 kV and 15 mA. The 2θ range was from 4° to 70°. For the measurement, around 1 g of sample was ground in an agate mortar, and the appropriate amount of powder (from both matrix and inclusion) was placed in a quartz sample holder and compressed with a glass slide. The MD Jade 9 software was used for the evaluation of the diffraction patterns and the identification of the mineralogical phases.

4.2 X-RAY MAPS

The maps were acquired by means of the SEM-EDS system installed in the laboratories of the Department of Earth Sciences in Turin using the AZTEC operating system of Oxford Instruments. Digital maps are made up of numerical matrices where in each pixel the number of X-rays detected for a particular characteristic energy interval for each mapped element is reported. TruMap © software has developed an algorithm for automatic peak deconvolution and background removal, thus allowing the real-time acquisition of compositional maps where each pixel corresponds to an X-ray spectrum with a net peak. This allows the easy processing of the map using the QUANTMAP©, which by processing the maps with a set of pre-acquired standards allows to obtain quantitative maps. The maps can be expressed as apparent concentration, percent by weight, atomic percent and percent of oxides.

The operating conditions were as follows: beam acceleration = 15 KeV, working distance = 10 mm, probe current = 5 nA. Using a process time of 1 µs these conditions have made it possible to reach approximately 100,000 counts per second (CPS) with a dead time of 30%. The maps were acquired at a fixed magnification of 50x. A dwell time of 7 ms was used which implies a total acquisition time of about 16 h for 8 frames scanned with a spatial resolution of 1024 X 768 pixels for a total of about 6.5 MPixel on 40 mm^2.

Each set of X-ray maps was corrected for instrument probe current drift due to long acquisition times by performing an automated measurement on a reference sample of known coordinates (x, y and z) at pre-set time intervals of 1 hour.

With these maps it was possible to: 1) - evaluate the porosity, the distribution of the aggregate within the binder and identify its mineral phases; 2) - perform a mapping to identify the value of the Hydraulic

Index of the two mortars; 3) - obtain a modal map of the mineral phases and other components present in the mortar.

5. Results

5.1 Petrography

In the following a petrographic description of the main features of the analyzed mortars is reported. In **Table 2** the main minerals and rock fragments that make up the aggregate are detailed for each sample.

Samples	Quartz	White Mica	Biotite	K-Feldspar	Plagioclase	Amphibole	Carbonate	Quartzite	Gneiss	Marble	Impure marble	Calcschist	Micaschist	Biotite bearing micaschist	Chlorite-schist	Graphite-schist	Serpentinite	Granitic Rock
ACK02	x	x		x	x			x										
ACK03	x	x		x				x	x		x			x				
ACK04	x	x		x		x		x					x					
ACK05	x	x		x	x		x	x	x	x	x		x			x		
ACK06	x	x		x	x				x		x			x		x		
ACK07	x	x		x	x	x	x	x	x		x	x		x		x		
ACK08											x							
ACK09	x	x		x				x	x			x			x			x
ACK10	x	x		x		x		x	x	x	x	x	x			x		
ACK11	x	x		x	x		x	x	x		x	x					x	
ACK12	x	x		x			x			x	x	x				x		
ACK13	x	x		x			x	x	x	x	x	x	x					
ACK14	x	x		x		x	x		x	x	x					x		
ACK15	x	x		x			x	x			x	x	x			x		
ACK16	x	x	x	x	x		x	x	x	x	x		x			x		x
ACK17	x	x		x		x	x	x	x									
ADY01	x	x		x	x	x	x			x		x	x			x		x
ADY02	x	x		x	x	x	x	x	x	x		x				x		x
ADY03	x	x		x	x	x		x		x	x		x		x	x		x
ADY04	x	x	x	x	x	x	x	x	x	x	x		x			x		x
ADY05	x	x	x	x	x	x	x			x	x				x	x		
ADY06	x			x		x		x	x	x	x		x			x		x
ADY07	x			x	x	x		x	x	x	x		x	x		x		
ADY08	x	x		x	x		x	x	x	x	x				x	x		
ADY09	x	x			x	x			x	x				x		x		
ADY10	x	x	x	x	x	x	x		x	x	x	x	x	x	x	x		x
ADY11	x		x	x	x	x	x	x	x	x		x			x			x
ADY12	x	x		x	x	x	x	x	x	x		x			x	x	x	x
ADY13	x	x		x	x		x	x		x	x	x				x	x	x

ADY15	x	x		x	x	x	x	x		x	x		x					
ADY16	x	x	x	x	x				x					x				x
ADY17	x	x	x	x		x	x	x	x	x	x			x	x	x		x
ADY18	x	x		x	x	x			x									
ADY19	x	x	x	x		x		x	x				x	x				
ADY20	x			x	x	x	x		x	x		x		x		x	x	
ADY21	x	x	x	x		x			x					x				

Table 2: Minerals and rocks present in Châtel Argent Castle samples (ACK) and in Quart Castle samples (ADY) respectively.

The aggregate has a granulometric distribution from serial to poorly classified. In almost all sections a bimodal particle size dispersion is observable. The smaller-grained portion of aggregate has dimensions ranging from submillimetric to about 2.5 mm and shapes from irregular to elongated and edges from sub-angular to sub-rounded, while the greater-grained portion is between 9 mm and 15 mm.

The composition is always heterogeneous, but with a silicate prevalence. In all sections there are clasts of quartz, especially in the fine-grained fraction of the aggregate. The edges can be both angular and rounded (**Figure 4a**). The most common rock fragments, in addition to single quartz crystals, are quartzites, with a fine and very fine grain. The quartzite elements appear for the most part with sub-spherical shapes and rounded edges. Very common are also the elements of white mica, which often occur in single crystals with a lamellar habit in the fine-grained fraction of the aggregate. Less abundant are biotite and chlorite. Both in the fine-grained and in the coarse fraction of the aggregate, there are elements of more or less altered feldspar with very fine-grained felts (**Figure 4a**). Locally, the polysynthetic twinning of plagioclase is recognized, or the Carlsbad twinning of potassium feldspar. Rock fragments of gneiss are frequently present (**Figure 4b**) composed mainly of fine-grained quartz and white mica oriented and distributed in levels that often envelop potassium feldspar porphyroclasts, often altered and medium-grained. Gneisses and quartzites usually constitute the elements of the aggregate with a coarser grain and have sub-angular and rounded edges (**Figure 4c**).

There are normally coarse-grained elements of impure marble composed of fine-grained carbonate crystals and minor quartz and fine-grained white mica oriented in discontinuous and not very thick levels. Frequently there are elements of the aggregate consisting of calcschist composed of fine-grained carbonate crystals, fine-grained white mica arranged in oriented levels of submillimeter and continuous thickness and less fine-grained quartz (**Figure 4b**).

Many samples include monocrystalline carbonate fragments that make up the fine-grained aggregate elements (**Figure 4b**). They often have angular or sub-angular edges and are interpreted as fragments of vein calcite added to the mixture. In some sections there are lithic elements of prasinite consisting of plagioclase, epidote, chlorite and actinolite, and elements of serpentinite consisting of serpentine and lesser magnetite (**Figure 4d**). Almost all sections contain graphitic schists, composed of thin and dense layers of white mica, graphite, and lesser quartz (**Figure 5a**).

Finally, there are lithic elements with a granite composition consisting of quartz, feldspar, and plagioclase as well as rare, isolated crystals of pyroxene and pleochroic amphibole from yellow to brown.

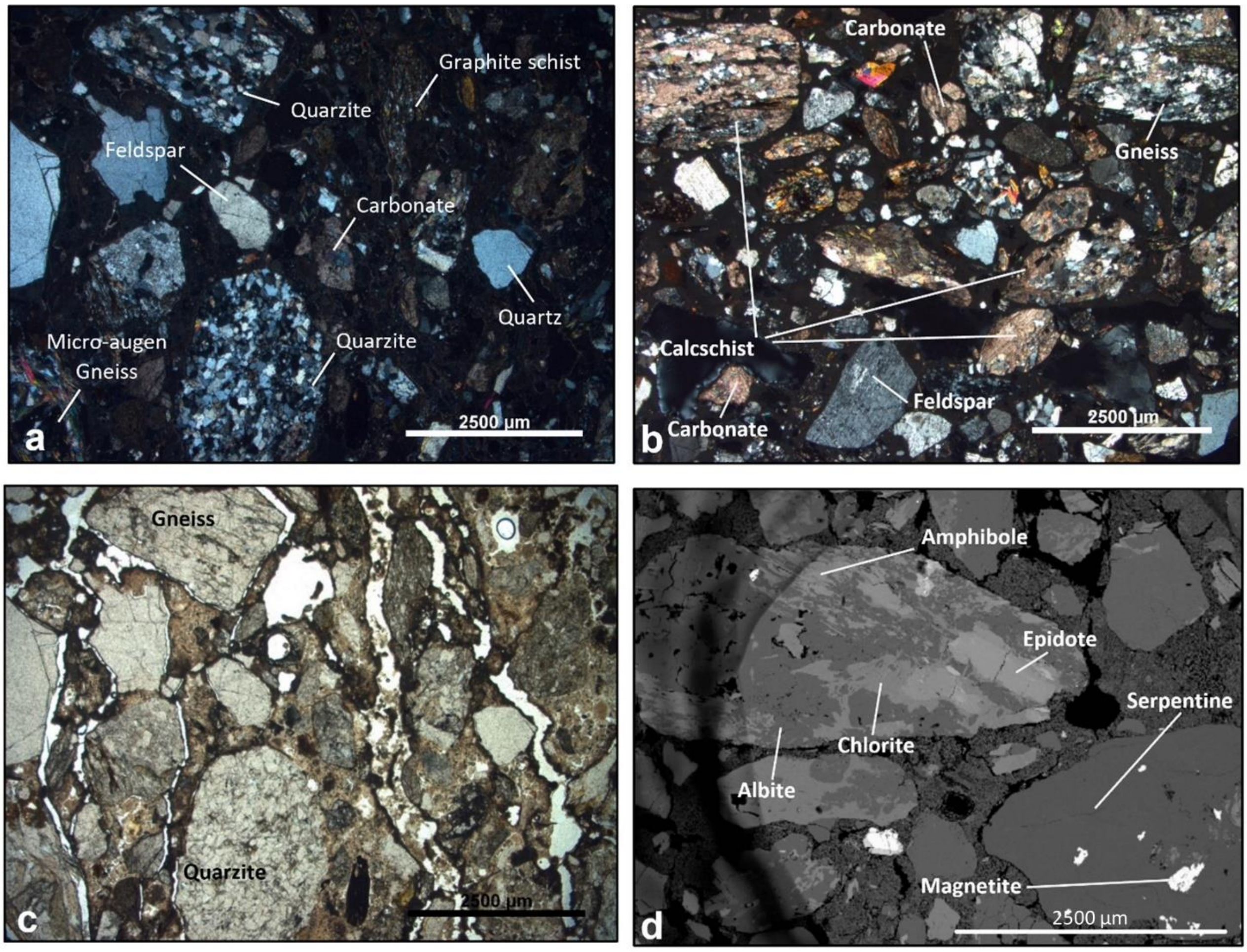

Figure 4: Micrographs of mortars: a) Crossed polarized light of ACK05 sample under optical microscope low resolution; b) Crossed polarized light of ADY02 sample; c) Plane polarized light of ACK05 sample: note the intense secondary porosity and the lower primary porosity; d) Photograph at SEM-EDS of ADY17 sample.

All sections show a slightly pervasive closed primary porosity (probably due to the use of excess water in the mixture, which creates bubbles) with rounded pores and dimensions ranging from sub-millimeter to a maximum of about 1.5 mm. In some samples these pores appear to be filled with re-precipitated minerals, probably of calcite composition. The secondary porosity, on the other hand, is due to shrinkage or degradation and proves to be more pervasive. Often this porosity develops from the primary one and determines the low degree of conservation of the mortars. In many cases the secondary porosity occurs along the edges of the aggregate elements, weakening the mechanical properties of the mortar (**Figure 4c**). In some sections, the secondary porosity presents fractures affecting the entire sample with spacing in the order of magnitude of 2 mm wide. Even along these fractures, precipitation recrystallization can be noted in some cases. The total porosity is estimated between 7% and 15% by volume.

In all samples some lumps are present. These are residues of raw material of the binder that did not react during cooking. They appear with rounded shapes and with sub-rounded to rounded edges, with dimensions ranging from submillimetric to about 3-4 mm. They have mostly homogeneous colours, dark brown or dark hazelnut, but especially in cases where the lumps are fractured (**Figure 5b**), they tend to be more intense in colour just along the edges, due to an incomplete reaction with the binder during cooking.

The ACK17 sample comes from a wall near the entrance to the castle cistern. The main feature of this sample is the presence of numerous inclusions consisting of fusion slag. These slags are formed by irregular fragments ranging in size from millimeters to micrometres in which a glassy portion is identified whithin skeletal crystals of wustite and olivine with a fayalite composition (**Figure 5c**). From their shapes and sizes, it can be deduced that they are slag generated during the iron extraction process, which in medieval times took place through the use of low-fire furnace that could reach 1200 °C. These elements were probably added to the mixture to make the binder no more aerial but hydraulic (see the SEM analyses) and thus make the mortar more resistant. This has also been achieved by adding artificial "cocciopesto" elements to the aggregate obtained from the mechanical crushing of bricks and other ceramic material, which at a macroscopic observation are brick red coloured. Finally, skeletal inclusions are worthy of note and are interpreted as remains of fossil coal combustion (**Figure 5d**).

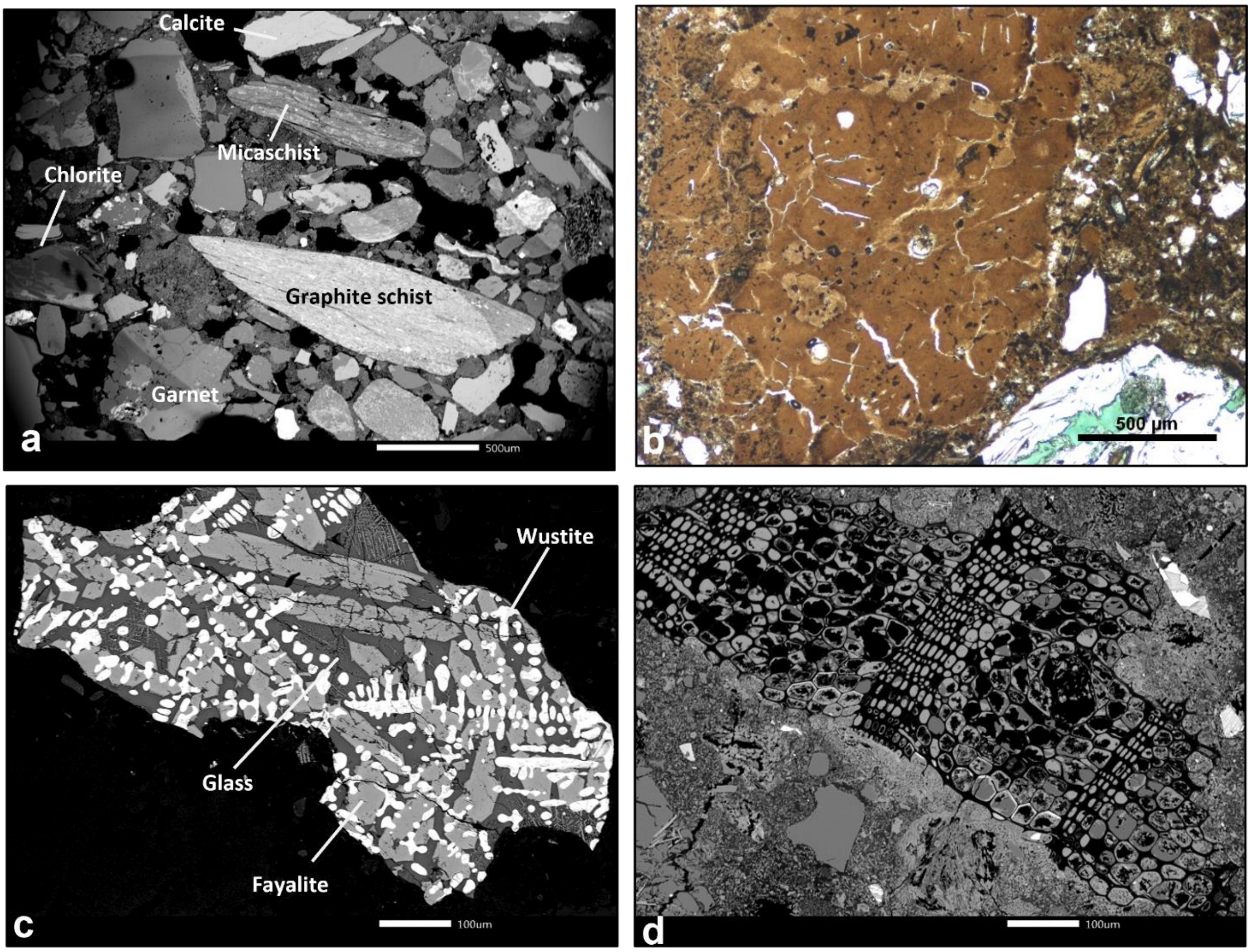

Figure 5: a) SEM photograph of the ADY04 sample; b) Plane polarized light microphotograph of ACK15 sample: note the intense fracturing of the lump; c) SEM photograph of ACK17 sample note the foundry waste with eutectic point structures; d) SEM photograph of sample ACK17; note the remnant fossil coal combustion.

5.2 Mineral chemistry

• *Pyroxenes:*

The pyroxenes come from single crystals present in the aggregate of the ACK04 and ACK12 samples from Châtel Argent and the ADY04 and ADY17 samples from the Quart Castle. The analyses were calculated on the basis of 6 oxygens and are available in supplementary materials (**Table S1**).

The pyroxenes were projected on the classification diagram of Morimoto (1988) (**Figure 6a**), and all show a calcitic composition. In particular, the samples fall into the fields of diopside-augite and pigeonite.

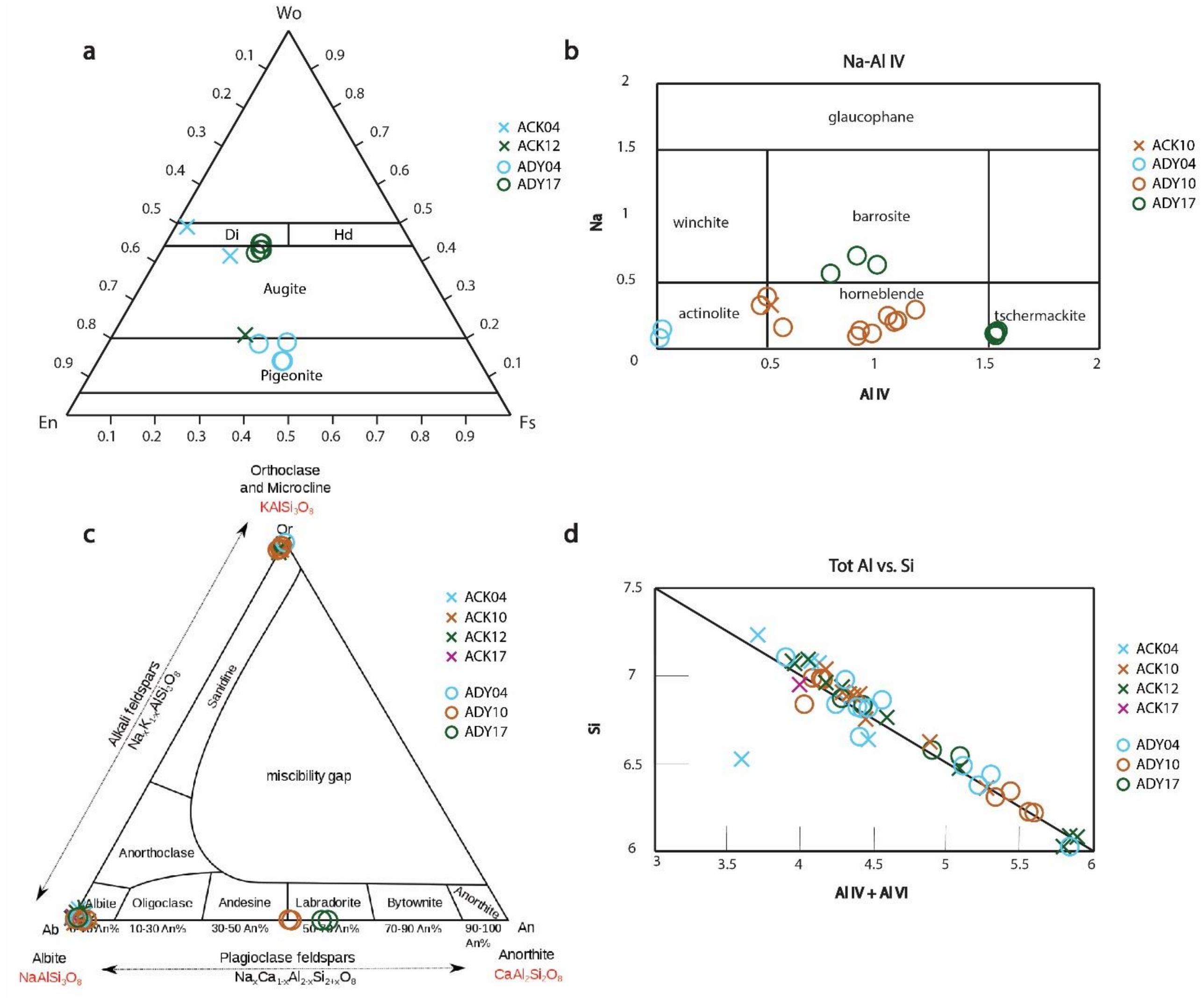

Figure 6: Different diagrams of samples of Châtel Argent and Quart Castle. a) Pyroxene ternary diagram (modified by Morimoto, 1988). En= Enstatite, Fs= Ferrosilite, Di= Diopside, Hd= Hedembergite, Wo= Wollastonite; b) Amphiboles; c) Feldspar diagram; d) Dioctahedral micas diagram.

The pyroxenes analyzed were therefore all calcic, while the typical sodium-calcium pyroxenes of the basic rocks equilibrated in eclogitic conditions of the Piemonte Zone and the sodium pyroxenes of the ortho-derivatives of the Sesia Lanzo Zone are missing. This data is consistent with the location occupied by the two castles studied, both placed to the west of the outcrop areas of the main eclogitic units of Aosta Valley. For the mortars of the Quart Castle, the pyroxenes identified could derive from the dismantling of basic rocks of a high metamorphic grade from the Valpelline Series: the attribution of the pyroxenes found in the mortars of the Châtel Argent Castle is more difficult. In this case it can be assumed that it comes from basic/ultrabasic rocks of the Versoyen Zone or from basic lenses of the polymetamorphic basement of the Gran St. Bernard multi-nappes system.

• *Amphiboles:*

The amphiboles derive from the ACK10 sample from the Châtel Argent site and from samples ADY04, ADY10 and ADY17 from the Quart Castle. The analyses were calculated on the basis of 23 oxygens and are available in the supplementary materials (**Table S2**).

The diagram which correlates the Na content of the M4 site, and the Al IV content was reported (**Figure 6b**). The amphibole of the ACK10 sample shows a composition that falls within the field of hornblende. The compositions of the ADY04 sample plot into the field of actinolite. The amphibole of the ADY10 sample shows different compositions, which fall into the fields of actinolite and hornblende, while those of the amphibole of the ADY17 sample plots into the fields of the barrosite and of the tschermackite. All the amphiboles analyzed can therefore be classified as calcium or sodium-calcium amphiboles with a composition ranging from tremolitic to pargasitic, reflecting conditions of medium-low pressure and variable temperature from low to medium metamorphic degree. Amphiboles of this type are present in numerous units of both oceanic and continental origin cropping out in the Aosta Valley, which have undergone a pervasive metamorphic retrogression under low pressure conditions, possibly with late heating. On the other hand, sodium amphiboles, characteristic of high pressures conditions, were absent. This data is consistent with the position occupied by the two castles studied, both located to the west of the outcrop areas of the main oceanic units of Aosta Valley, which suffered eclogitic facies conditions.

•*Feldspars:*

The feldspars analyzed come from the ACK04, ACK10, ACK12 and ACK17 samples from Châtel Argent Castle and from the ADY04, ADY10 and ADY17 samples from the Quart Castle and refer to aggregate elements consisting of lithic fragments, or single clasts of feldspar. The analyses were calculated on the basis of 8 oxygens and are available in supplementary materials (**Table S3**) and are represented in the diagram of **Figure 6c**.

The composition of feldspars is variable and can be summarized in three categories:

- Albite: all the analyses carried out on the ACK04 and ACK17 samples plot into this field, together with some of the ACK10 and ACK12 samples and the ADY04, ADY10 and ADY17 samples. These compositions are typical of Aosta Valley rocks of greenschist metamorphic grade originating from both the basic and pelitic protolites.

- Orthoclase: an analysis of the ADY04 sample falls on the vertex of the field, while the feldspar of the ACK10, ACK12 and ADY10 samples are arranged along the Ab-Or side, with approximately a maximum 7% of albitic molecule. The presence of K-feldspar can be attributed to orthogneiss dismantling materials (in most cases) widespread in the continental units of Gran Paradiso, Monte Rosa and Gran St. Bernard or granite (most likely coming from the erosion of the Mont Blanc granites).

- Labradorite: the analyses of the ADY10 and ADY17 samples plot on the Ab-An side between 52 % and 60% of anorthitic molecule. Intermediate composition plagioclases could come from basic rocks or from high temperature units, such as the Valpelline Series.

• *Dioctahedral micas:*

The dioctahedral micas come from single crystals dispersed in the binder and from micas present in lithic fragments in the aggregate of samples ACK04, ACK10, ACK12 and ACK17 of the Châtel Argent Castle and of the samples ADY04, ADY10 and ADY17 of the Quart Castle. The analyses were calculated on the basis of 22 oxygens and are available in supplementary materials (**Table S4**).

Almost all of the micas analyzed appear to belong to the family of potassic micas (muscovites), while only a few samples belong to the family of paragonitic micas.

The micas of the ACK04, ACK10, ACK12 and ACK17 samples are reported in the diagram Al tot / Si (**Figure 6d**), which allows a subdivision in almost pure muscovite and in terms close to the phengite composition. The analyses are distributed approximately along the Muscovite-Phengite junction.

The micas analyzed therefore reflect high pressure metamorphic conditions, typical of the continental crust units outcropping in Aosta Valley and, in particular, in the eclogitic facies units such as the Gran Paradiso massif and those in blueschist facies of the Gran St. Bernard multi-nappe system.

•*Trioctahedral micas:*

The trioctahedral micas come from single crystals occurring in the aggregate of samples ADY04, ADY10 and ADY17 of the Quart Castle. The analyses were calculated on the basis of 22 oxygens and are available in supplementary materials (**Table S5**).

The biotites likely come from high temperature metamorphic lithotypes, such as the kinzigites of the Valpelline Series.

5.3 Analyses of binders

The composition of the binders was performed on six thin sections: three relating to the Châtel Argent Castle (ACK10, ACK12 and ACK17) and three relating to the Quart Castle (ADY04, ADY10 and ADY17). The following description of the binders has been divided according to their use, so as to highlight the differences in composition. The results are expressed as wt%.

The first group of binders comes from Quart Castle. All three analyzed samples derive from plasters, the analyses of their binders can be consulted in **Table 3**.

Sample	*SiO_2*	*Al_2O_3*	*Fe_2O_3*	*MgO*	*CaO*	*H.I.*
ADY04_1	3.15	1.34	0.00	42.59	52.67	0.047
ADY04_2	5.89	2.35	0.00	39.43	51.15	0.091
ADY04_3	1.03	0.00	0.00	42.26	46.71	0.010
ADY04_4	2.43	1.16	1.08	42.68	52.65	0.049
ADY04_5	3.27	1.76	0.72	44.75	48.97	0.061
ADY04_6	3.61	1.08	0.00	36.65	58.36	0.049
ADY04_7	1.26	0.00	0.00	37.42	61.32	0.013
ADY04_8	4.72	1.29	0.00	41.96	51.71	0.064
ADY04_9	3.52	1.36	0.69	43.37	50.37	0.059

ADY04_10	2.47	0.00	0.00	47.12	49.88	0.025
ADY10_1	6.27	3.31	1.27	33.39	53.18	0.125
ADY10_2	3.30	0.00	0.00	37.58	57.44	0.035
ADY10_3	3.53	0.00	0.00	35.29	59.51	0.037
ADY10_4	2.70	1.14	0.00	33.00	61.16	0.041
ADY10_5	1.86	0.00	0.00	40.04	50.38	0.019
ADY10_6	2.92	2.82	0.00	42.04	50.38	0.062
ADY10_7	2.98	1.10	0.00	36.77	56.54	0.044
ADY10_8	2.85	1.17	0.00	38.39	55.11	0.043
ADY10_9	3.00	1.18	1.54	36.14	56.28	0.062
ADY10_10	2.46	0.00	0.00	39.20	56.01	0.026
ADY17_1	8.88	1.95	0.82	44.79	45.55	0.132
ADY17_2	4.03	1.16	0.00	39.51	55.30	0.055
ADY17_3	3.45	1.54	0.00	41.45	53.56	0.053
ADY17_4	8.97	0.96	0.00	42.05	48.03	0.110
ADY17_5	6.88	2.63	1.12	40.87	47.82	0.120
ADY17_6	7.75	1.35	0.00	41.52	49.37	0.100
ADY17_7	1.82	0.54	0.00	12.90	84.50	0.024
ADY17_8	1.31	0.00	0.00	11.18	86.67	0.013
ADY17_9	0.93	0.00	0.00	13.79	84.98	0.009
ADY17_10	6.88	0.00	0.00	24.43	68.69	0.074
ADY17_11	3.99	0.00	0.00	27.17	68.48	0.042
ADY17_12	6.22	0.91	0.00	49.85	42.61	0.077
ADY17_13	4.42	0.00	0.00	49.06	46.51	0.046
ADY17_14	4.31	1.21	0.00	40.48	53.67	0.059
ADY17_15	3.91	1.01	0.00	38.18	56.90	0.052

Table 3: Analyses of binders from the plasters of Quart Castle. Acronyms represent percentage weight of oxides and H.I. the Hydraulic Index.

In most cases, the binder is magnesian and therefore with a high MgO component that varies between 24.43% and 49.85%, while the calcic component varies between 42.61% and 68.69%. Only three samples show a MgO percentage between 11.18% and 13.79%, while the CaO percentage varies between 84.50% and 86.67%. SiO_2 values are low and vary between 0.93% and 8.97%, Al_2O_3, not always present, has values between 0.91% and 3.31%, while Fe_2O_3, is in most cases absent, reaches up to 1.54%. The Hydraulic Index (H.I.) identifies an aerial binder (see **Table 3**) with values ranging from 0.010 to 0.091 for mainly samples. Only five samples from ADY17 sample show H.I. values between 0.100 and 0.132 which identifies weakly hydraulic binders.

The ADY04 samples have a homogeneous binder, which generally shows a composition made up in a minimal part also of potassium (maximum 1.75%).

ADY10 section has different sites that present higher values of SiO_2, while CaO and MgO values are almost stable.

Numerous sites were analysed in the ADY17 section and many of them present different ranges of values, expecially the SiO_2 ones.

The second group of binders comes from Châtel Argent Castle. The ACK10 and ACK12 samples come from the external walls of the castle, while the ACK17 sample comes from the masonry of the water tank inside the external walls. The analyses of their binders are reported in **Table 4**.

Sample	*SiO_2*	*Al_2O_3*	*Fe_2O_3*	*MgO*	*CaO*	*H.I.*
ACK10_1	22.54	6.38	2.79	3.69	63.12	0.475
ACK10_2	21.37	7.31	2.57	5.03	61.74	0.468
ACK10_3	24.02	5.43	2.39	5.27	61.40	0.478
ACK10_4	25.18	5.89	1.42	6.05	58.68	0.502
ACK10_5	15.45	4.11	3.61	5.00	71.05	0.305
ACK10_6	19.57	7.25	2.15	3.29	66.00	0.418
ACK12_1	4.20	0.00	0.00	3.39	92.41	0.044
ACK12_2	4.97	0.99	0.00	3.12	90.93	0.063
ACK12_3	9.98	3.48	1.38	4.31	80.40	0.175
ACK12_4	9.54	4.39	2.88	6.38	76.61	0.203
ACK12_5	9.40	2.99	1.35	3.09	83.17	0.159
ACK12_6	11.55	5.60	1.25	3.51	76.80	0.229
ACK12_7	6.95	1.33	0.95	5.61	85.15	0.102
ACK12_8	10.38	2.22	0.89	6.04	80.09	0.157
ACK12_9	6.63	2.15	0.92	2.62	87.00	0.108
ACK17_1	40.14	8.88	2.42	4.23	44.33	1.059
ACK17_2	36.18	8.14	6.25	3.95	45.48	1.023
ACK17_3	39.12	8.55	2.20	4.72	45.41	0.995
ACK17_4	36.98	10.21	2.15	3.67	46.99	0.974
ACK17_5	31.29	10.07	2.06	8.52	48.05	0.768
ACK17_6	32.42	8.24	3.82	5.45	49.14	0.815

Table 4: Analyses of binders from the plasters of Châtel Argent Castle. Acronyms represent percentage weight of oxides and H.I. the Hydraulic Index.

For the ACK10 and ACK12 samples the composition is generally calcic (the values of CaO vary from 58.68% to 92.41%), with SiO_2 values ranging from 4.20% to 25.18%, MgO between 2.62% and 6.38%. Al_2O_3 and Fe_2O_3 are present in most of the analyses in quantities respectively between 1.33% and 7.31% and between 0.89% and 3.61%. The ACK17 sample shows a marly composition (respectively with values between 44.33% - 49.14% for CaO and 31.29% - 40.14% for SiO_2) with lower MgO (3.95%-8.52%), Al_2O_3 between 8.14% and 10.21% and Fe_2O_3 between 2.06% and 6.25%. The Hydraulic Index varies for the different sections. In the ACK10 sample the binder has an average value ranging from properly hydraulic (H.I. = 0.305) to eminently hydraulic (H.I. = 0.502) and shows a coarse grain (up to about 50 µm) with an important microporosity.

The ACK12 sample shows two different binders, distributed in bands. One has a micritic grain and a lower Hydraulic Index, with values ranging from 0.044 to 0.063 and is identified as an aerial binder, while the other has a microsparitic appearance (with greater grain), where white mica crystals are abundant and with values of H.I. ranging from 0.102 to 0.229 (medium to properly hydraulic binder).

The binder of the ACK17 sample has an uneven grain and is microfractured. Its Hydraulic Index is high and varies from 0.768 to 1.059, identifying no longer as lime, but as cement. The presence of a high amount of silicon in its composition was probably intended to allow the mortar to have a hydraulic setting process considered for its use in the water tank. In this case the binder shows an important shrinkage microporosity.

XRPD analyses performed on two representative samples (ADY10 and ACK17) confirmed the overall mineralogical pattern identified by the SEM-EDS facility for both castles (Figure 7a and Figure 7b). In particular, in the Quart Castle sample the occurrence of dolomite is reported, absent in the Châtel Argent Castle sample. The occurrence of akermanite in the ACK17 can be related to the activation of reaction between blastofurnace slag and carbonate minerals (calcite or dolomite) during the baking process.

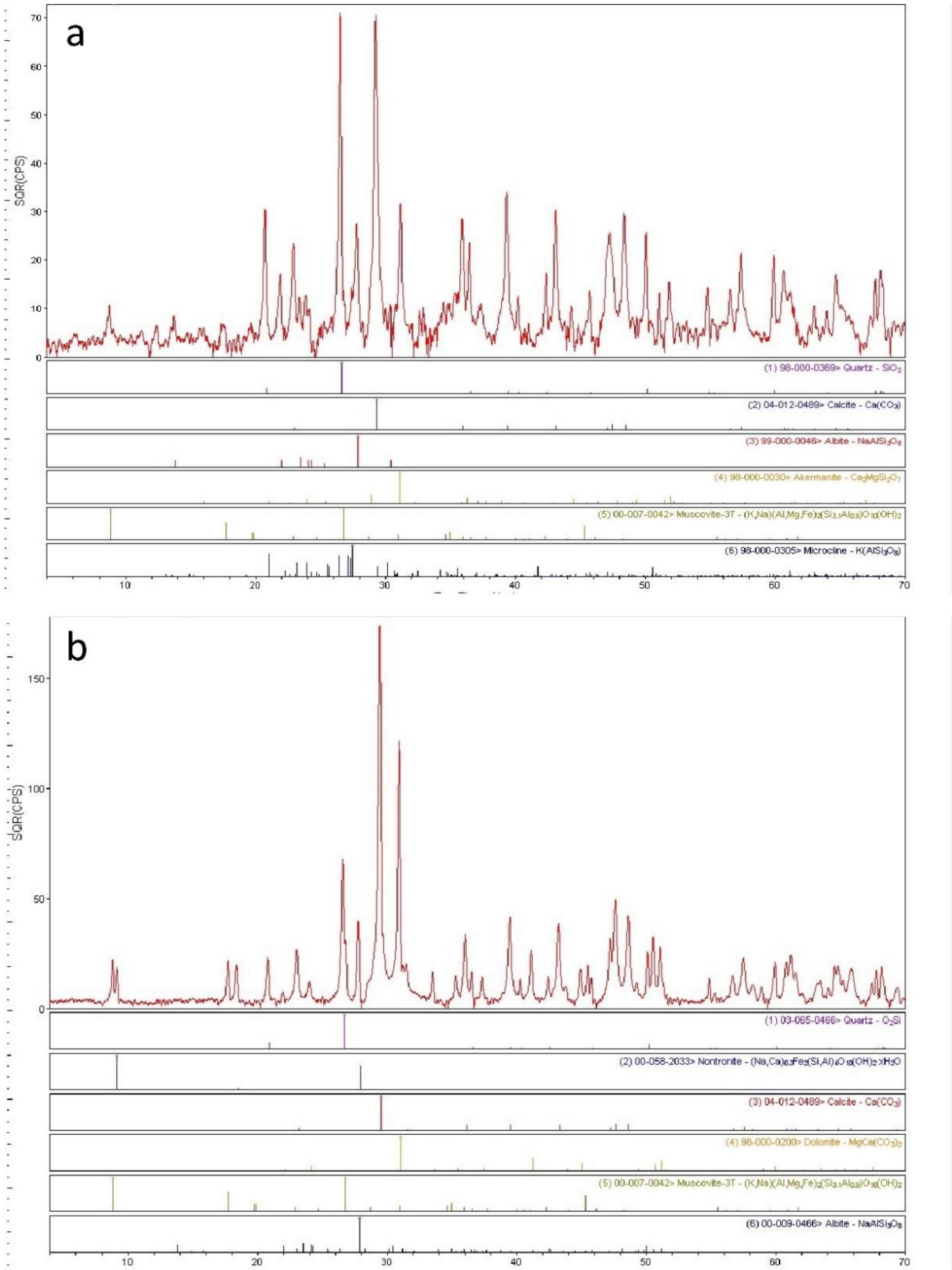

Figure 7: XRPD analyses of ADY10 sample (a) and ACK17 sample (b).

5.4 X-ray maps

The overall observation of the maps made it possible to provide some information relating to the various components of the mortar investigated. For example, the binder / aggregate ratio, the shape and distribution of the elements of the aggregate, the shape and distribution of porosity can be appreciated.

In **Figure 8** the quantitative maps of the main oxides (SiO_2, Al_2O_3, CaO, MgO, Na_2O, K_2O) of the ADY17 section are represented, divided into discrete classes with false colours. The data are reported as Wt % of the oxide. The comparison of the maps allows to identify the different mineral phases that make up the aggregate of the mortar. The main distinguishable phases are (in order of abundance): quartz, albite, potassium feldspar, calcite, dolomite, white mica, chlorite and titanite. All clasts show an average size below 1 mm and a fairly homogeneous grain, with some larger lithic clasts. Their shape is generally rounded and sub-spherical. Among the feldspar there are both albite and K-feldspar. Phyllosilicates (white mica and chlorite) are relatively abundant.

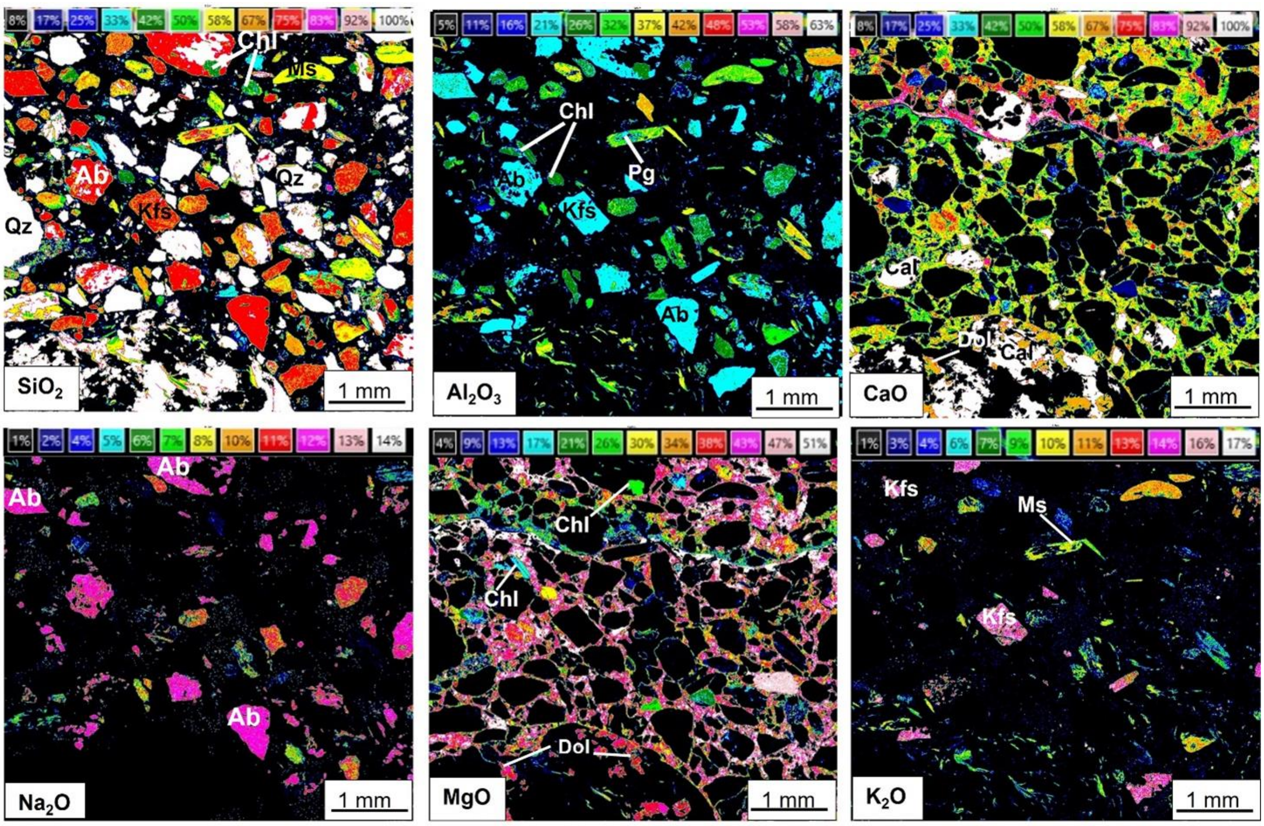

Figure 8: Quantitative maps of the main oxides found in the ADY17 section of Quart Castle. The legend refers to intervals of discrete percentage expressed in false colours. Ab= Albite, Cal= Calcite, Chl= Chlorite, Dol= Dolomite, Kfs= K-feldspar, Pg= Paragonite, Ms= Muscovite, Qz= Quartz (Mineral abbreviations according to Whitney and Evans, 2010).

As regards the binder, it can be observed that its composition is slightly inhomogeneous and composed mainly of CaO and MgO.

Figure 9, on the other hand, shows the quantitative maps of the main oxides (SiO_2, Al_2O_3, MgO, CaO, Na_2O, FeO) of the ACK17 section. This section shows the particularity of being made up of an aggregate composed of natural materials (silicate mineralogical phases) and artificial materials with pozzolanic behavior, such as the slag from iron processing (aggregates of fayalite, wustite and glass that are clearly distinguishable in the map of the iron) and fragments of cocciopesto, easily recognizable by comparing the maps of silicon and aluminum. The main components of the aggregate are (in order of abundance): cocciopesto, quartz, albite, melt waste, combustion residues (coal), chlorite, light mica and rare carbonate. From the comparison between the various maps, it can be seen that the larger lithic clasts are made up of schists fragments composed by white mica, chlorite and quartz (in the central portion on the right of the map), followed by albite, which is present in submillimeter clasts and quartz in very small fragments.

The binder is mainly calcic with a minor magnesium component of the previous section, while the presence of phyllosilicates is clearly visible. There are also abundant shrinkage microfractures, which appear to be filled with re-precipitated carbonate. On the other hand, primary porosity is practically absent.

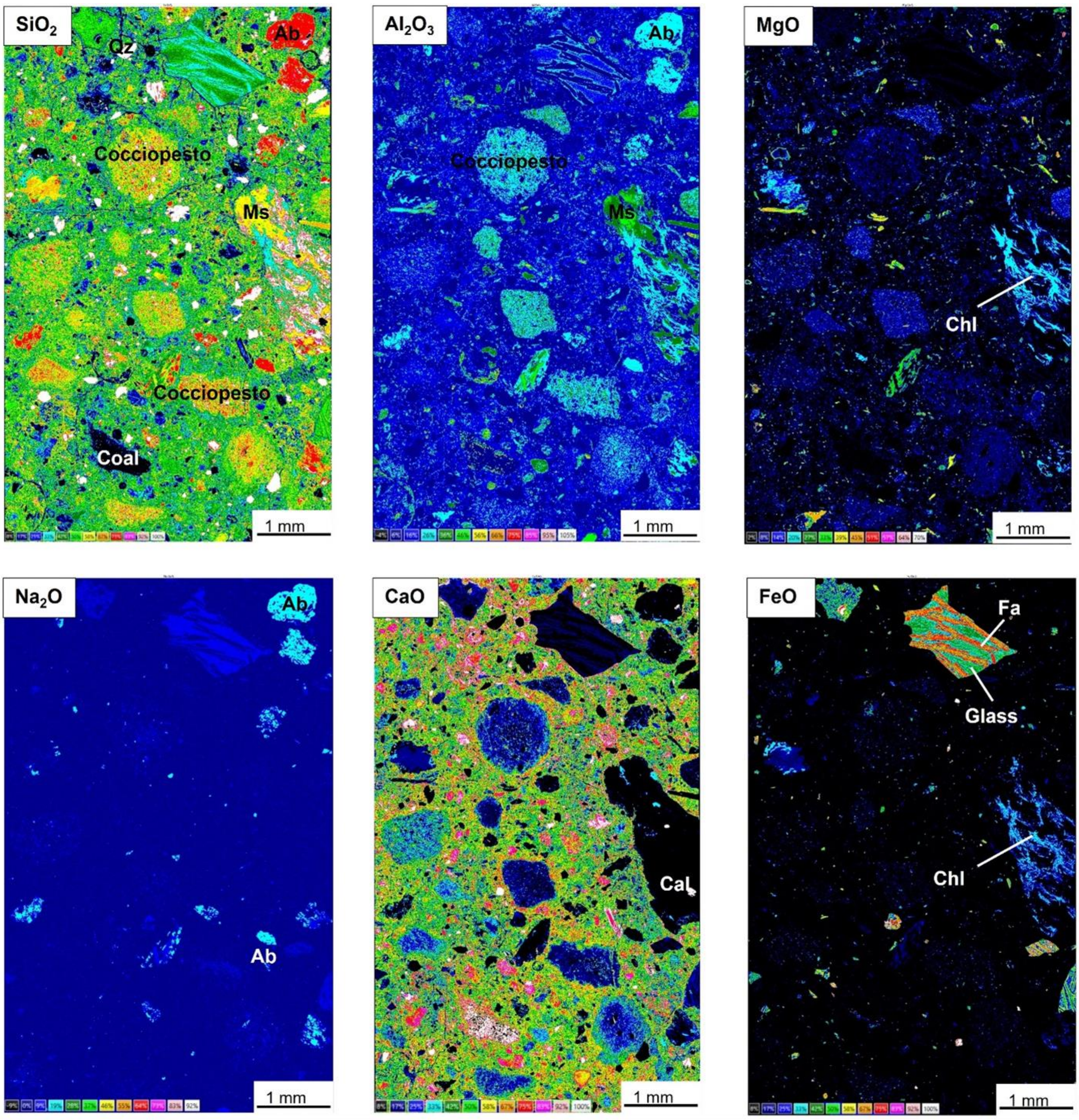

Figure 9: Quantitative maps of main oxides found in the ACK17 section of Châtel Argent Castle. The legend refers to ranges of discrete percentages expressed in false colours. Ab= Albite, Cal= Calcite, Chl= Chlorite, Fa= Fayalite, Ms= Muscovite, Qz= Quartz (Mineral abbreviations according to Whitney and Evans, 2010).

The modal compositional maps sections and their relative legends expressed in false colours are shown in **Figure 10** (ADY17) and **Figure 11** (ACK17), processed through the MultiSpec© program (Multispectral Image Data Analysis System) (Biehl and Landgrebe, 2002).

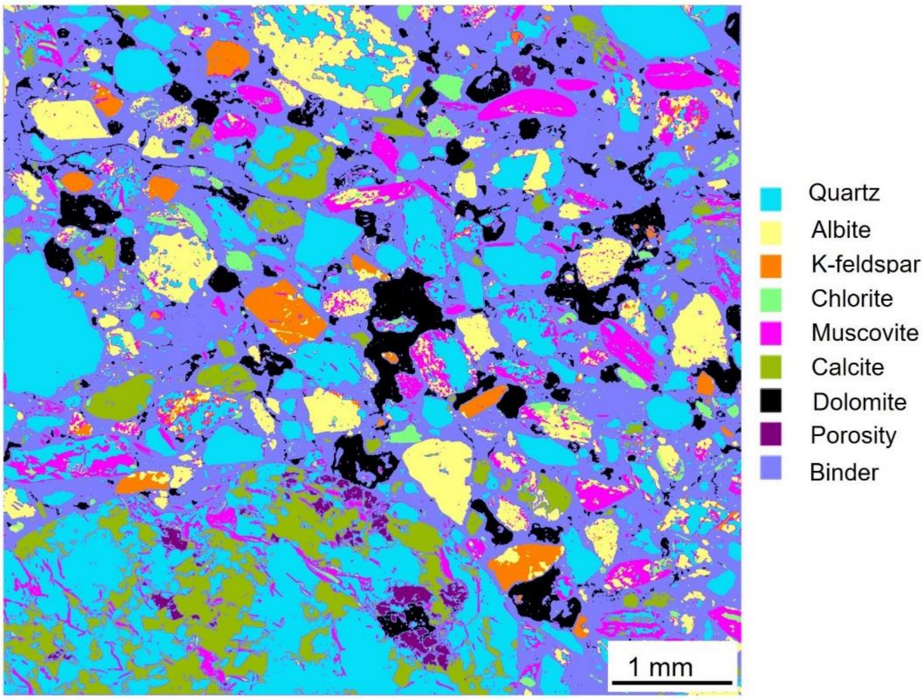

Figure 10: Modal compositional map of ADY17 section of Quart Castle.

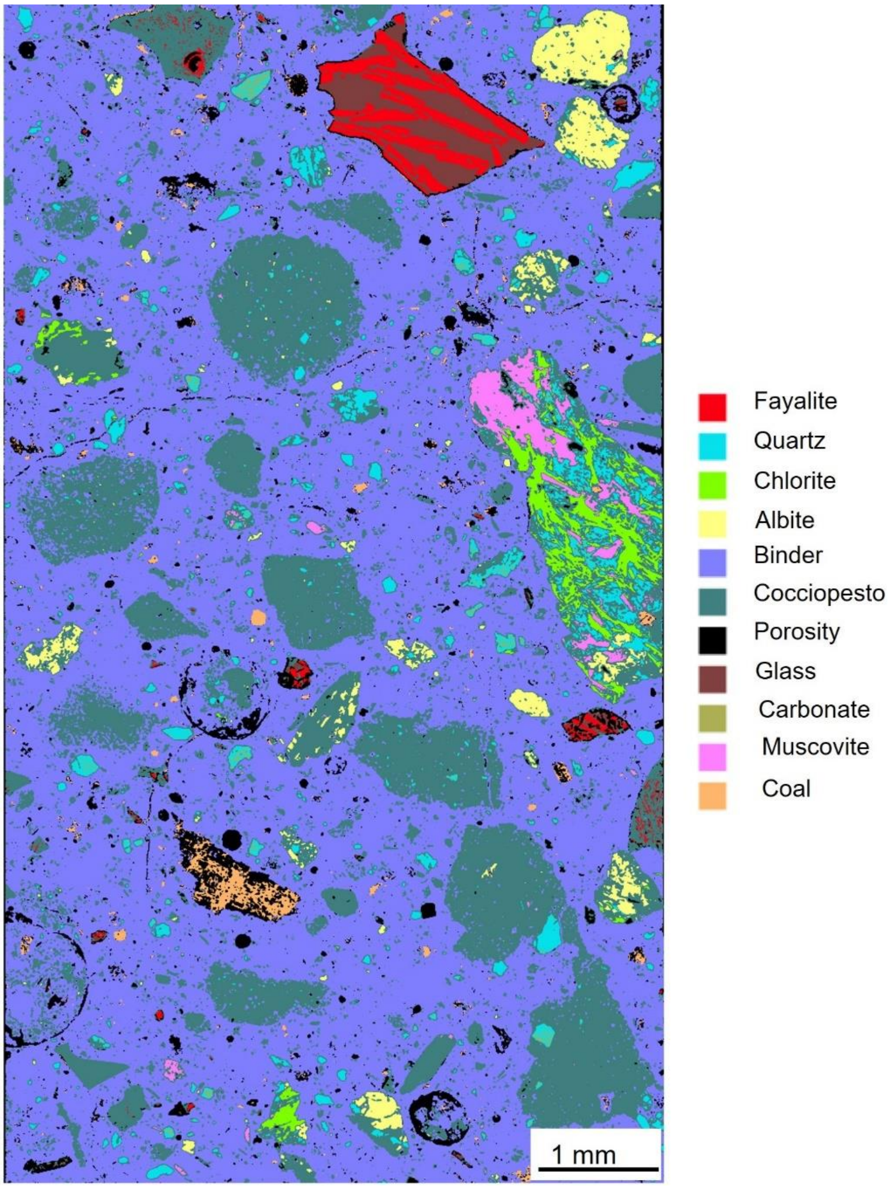

Figure 11: Modal compositional map of ACK17 section of Châtel Argent Castle.

This maps processing allows to calculate the percentage quantity of the single phases present in the samples, which in this case are respectively reported in **Table 5** (relative to the data of the ADY17 section) and **Table 6** (relative to the data of the section ACK17).

It can be noted that in both sections the binder is the most abundant phase, with a value of 38.21% for the ADY17 section and 60.86% in the ACK17 section. Another interesting information that this processing method can provide is the percentage value of the porosity. For the ADY17 sample it is around 7.31%, while for the ACK17 it stands at 3.93%. From the observation of the two modal maps, it can also be deduced that in the first case the primary porosity is concentrated in subspherical pores of irregular shapes and not communicating with each other, in the second case mainly secondary porosity occurs, due to shrinkage phenomena. The percentage of inert material is equal to 54.48 for the ADY 17 section and 35.21 for the ACK 17 section. From here it can be deduced that the binder / aggregate ratio is 0.70 for the mortar of the Quart Castle, a very low value, also considered that it is a plaster mortar and 1.73 for the mortar of the of Châtel Argent Castle.

Class	*Percent*
Quartz	24.74
Albite	9.27
K-feldspar	2.29
Chlorite	1.73
Muscovite	8.26
Calcite	7.32
Dolomite	0.86
Porosity	7.31
Binder	38.21
Total	100.00

Table 5: Values percentages of the phases present in section ADY17 of Quart Castle.

Class	*Percent*
Fayalite	1.31
Quartz	2.48
Chlorite	1.16
Albite	1.96
Carbonate	0.20
Muscovite	0.93
Coal	0.86
Cocciopesto	24.94
Porosity	3.93
Binder	60.86
Total	100.00

Table 6: Values percentages of the phases present in section ACK17 of Châtel Argent Castle.

The aggregate component of the ADY17 mortar consists mainly of quartz with a percentage of 27.74%, there are also albite at 9.27%, muscovite at 8.26% and calcite at 7.32%, in low quantities there are also potassium feldspar (2.29%), chlorite (1.73%) and dolomite (0.86%).

For the mortar of the ACK17 sample, the aggregate is mainly formed by fragments of cocciopesto with a value of 24.94%, followed in very low percentages by quartz (2.48%), albite (1.96%) an amorphous phase (glass) (1.38%) and fayalite (1.31%) which together constitute the smelting slag from iron processing (2.69%), followed by chlorite with a value of 1.16%, muscovite (0.93%), remains of coal (0.86%) and carbonate (0.20%).

5.5 Hydraulic index map

An important parameter to which reference for the analysis of mortars is the Hydraulic Index (H.I.). This index is strictly related to the quantity of clayey minerals or hydraulicizing materials that are part of the starting composition of the binder. It is identified by the formula:

$$I = \frac{SiO_2 + Al_2O_3 + Fe_2O_3}{CaO + MgO}$$

The numerator indicates the acid components of the binder, while those with the denominator, its basic components. Based on the value of the Hydraulic Index, the binders can be distinguished according to the following classification (**Table 7**) by Mariani (1976):

Lime	*Weakly Hydraulic*	*Medium Hydraulic*	*Properly Hydraulic*	*Eminently Hydraulic*	*(Cements)*
Hydraulic Index	0.10-0.16	0.16-0.31	0.31-0.42	0.42-0.50	0.50-0.65

Table 7: Classification of binders, by Mariani (1976).

Figure 12 and **Figure 13** show the maps of the Hydraulic Index, respectively, of sections ADY17 and ACK17. The maps were constructed by means of a simple algebraic operation, using the numerical matrices of the quantitative maps of Al_2O_3, Fe_2O_3 and SiO_2 at numerator and the acquired maps of CaO and MgO at denominator. In this way, the complete quantification point by point of each EDS spectrum (expressed as oxides) of the map was performed, in order to calculate the distribution of the Hydraulic Index (H.I.), with its statistical error, within the mapped area. The values obtained were then divided into discrete classes, reported in the legend and graphed using false colours. It can be noted that the intervals of the selected classes are not constant but reflect the one generally used for the classification of mortars reported in **Table 7**.

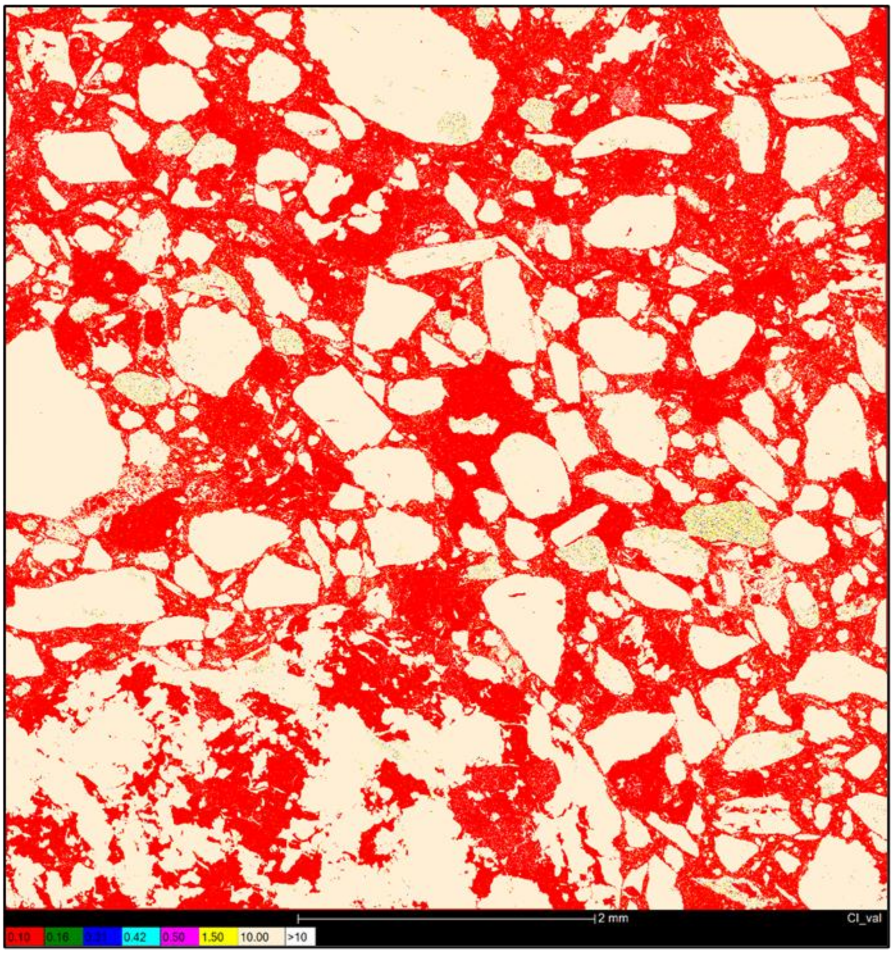

Figure 12: Map of Hydraulic Index value of ADY17 section (Quart Castle).

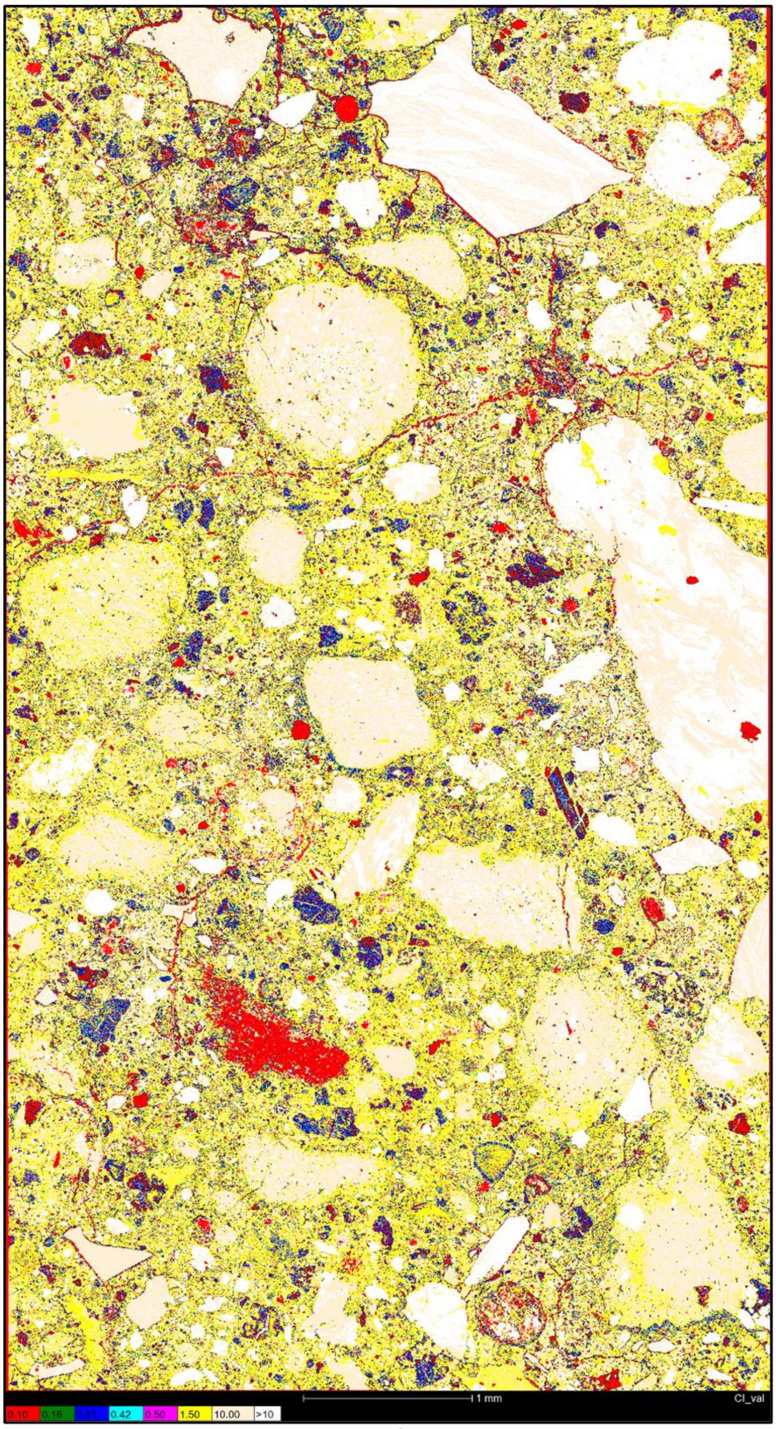

Figure 13: Map of Hydraulic Index value of ACK17 section (Châtel Argent Castle).

The value of the Hydraulic Index is uniform and ranges between 0.00 and 0.10 for the ADY17 section, allowing to deduce that the binder is very homogeneous and of the aerial type (H.I. < 0.10). Those values are concordant with the values got through the microprobe analyses which are between 0.009 and 0.132 (**Table 3**). This indicates that in the preparation of the binder, in the specific case of magnesian composition due to the composition reported in **Table 3,** no hydraulic additives were added and therefore the setting took place through the typical exchange reaction between the CO_2 of the atmosphere and the H_2O of the binder:

$$Ca(OH)_2 + CO_2 > CaCO_3 + H_2O \quad \text{or} \quad Mg(OH)_2 + CO_2 > MgCO_3 + H_2O$$

As for the ACK17 section, the value of the Hydraulic Index is more inhomogeneous, indicating that the binder also has a heterogeneous composition, perhaps accentuated by its coarser grain.

The calculated Hydraulic Index resulted between of 0.50 and 1.50 values, corresponding to a binder that ranges from eminently hydraulic to decidedly cement and concordant with the values analyzed through the microprobe analysis which are between 0.768 and 1.059 (**Table 4**). A deliberate selection of the aggregate nature and grading to contribute to mortar impermeability was also applied for the cistern in Amaiur Castle (Navarre, Spain), where ceramic and silico-aluminous rock fragments were used as aggregates tank to confer hydraulicity to the mortars (Ponce-Anton et al., 2020).

The presence of an important microfracturing is also highlighted by the widespread red veins (carbonate in composition) due to the cementitious character of the binder and therefore less plastic than less hydraulic binders.

6. Discussion

In this paper an analytical protocol based on a complete minero-petrographic approach for the study of medieval castles mortars from Aosta Valley (NW Italy) is reported. This method requires time to collect X-ray maps of the sections to be analyzed, and then to process the collected data; but it allow to define different features of a mortar as the chemical composition of aggregates and binder (reported as Wt % of single oxides present), the percentage of porosity and its distribution, and the aggregates/binders ratios. The aggregate is defined by the petrographic approach through the study of rocks fragments and minerals, so the mineral phases compositions are characterized by the EDS analyses, in such a way to define the area of provenance of the raw materials used to make the mortars.

Similar analytic approach was reported by Carò et al. (2008), which studied plasters and mortars from medieval Lardirago Castle (Pavia, northern Italy) by means of petrographical and chemical analyses. Similar conclusions were reported. Two main types of binders were available: pure lime and magnesian lime; neither hydraulic binders nor additives have been employed. The most ancient building phase, which dates back to the 12th century, is characterized by the use of magnesian limes for both plaster and mortar mixtures. The mineral composition of the aggregate correspond to lithic sand of fluvial origin.

According to the data reported in the previous chapters, the mortars of the two castles under analysis differ on several aspects.

The mortars sampled from the Châtel Argent Castle (ACK) generally show a higher quantity of binder than the one present in the mortars from the Quart Castle. In fact, the former has a binder / aggregate ratio (B / A) generally of 1/3 and in some cases of 1/2 or 1/4. The mortars from Quart Castle (ADY) show an B / A ratio generally around 1/5, except for some sections that have values of 1/4 or 1/6.

The two binders are also very different compositionally: in particular the composition of the binder used in the mortars of the Châtel Argent Castle (from the end of the 13th century) was calcic, with values of CaO that varies from 58,68% to 92.41%, while the MgO values varies from 2.62% and 6.38%. In the Quart Castle mortar (sample) (from the end of the 12th century) the composition of the binder was magnesian, with CaO values varies from 42.61% and 68.69% and MgO values between 24.43% and 49.85%. This diversity could be explained by petrographic considerations. The Quart Castle is in fact located a few hundred meters from strongly tectonized meta-dolostone belonging to the Roisan Zone, corresponding to the Mesozoic cover of the Mont Mary nappe and outcropping along the bed of the Bouthier Stream. It is therefore possible that the workers of the time used this material to prepare the binder used in the Castle.

The use of magnesian mortars in medieval times was rather limited. For example, the ancient mortar employed in the medieval port of Genova were found to be produced with magnesian lime (Mannoni, 1988). In many other cases the mortar binder used in medieval castles of Aragon (Ponce-Antón et al., 2021) and Andalusia (Cosano et al., 2021) was found to be made of lime.

The total porosity varies between percentage values of 7% and 15% for the Châtel Argent Castle sections represented by mostly primary and close porosity due to bubbles of air present in the mixture, and between 8% and 20% for the Quart Castle sections, where the secondary porosity due to shrinkage are more common and sometimes it is spread to the entire section. In the Quart Castle samples, the primary porosity is also relevant and it can contribute to develop a serious secondary porosity. The presence of higher MgO values in the Quart Castle samples tend to reduce the strength in the mortar because of the behavior of the magnesian binder during the drying process, which create a capillary stress around the primary porosity and produce the shrinkage. A high degree of pore interconnection, high desorption index and the presence of high pore volume in the 0.01 µm to 1 µm size range affect the mortar durability since pores retain water longer inside the mortar.

6.1 Petrographic considerations and geological correlations

The mineralogical composition of the aggregate of the two different sites studied and some of its characteristics reflect the lithologies found in the areas adjacent to the two castles.

In particular, it can be noted that biotite is generally present in the samples of the Quart Castle and only in one sample of the Châtel Argent Castle. Precisely, biotite in the Aosta Valley can be easily traced back to the dismantling of the kinzigites belonging to the Valpelline Series, dismantled and transported downstream by the Buthier Stream, a left tributary of the Dora Baltea River, where it flows into the city of Aosta, that is just upstream of the site where the Quart Castle is located (**Figure 14**).

The few glaucophane crystals present in the sections of the Quart Castle could derive from the eclogitic units that outcrop south of Quart on the orographic right of the Dora Baltea River, as well as the clasts of serpentinite and prasinite (**Figure 14**).

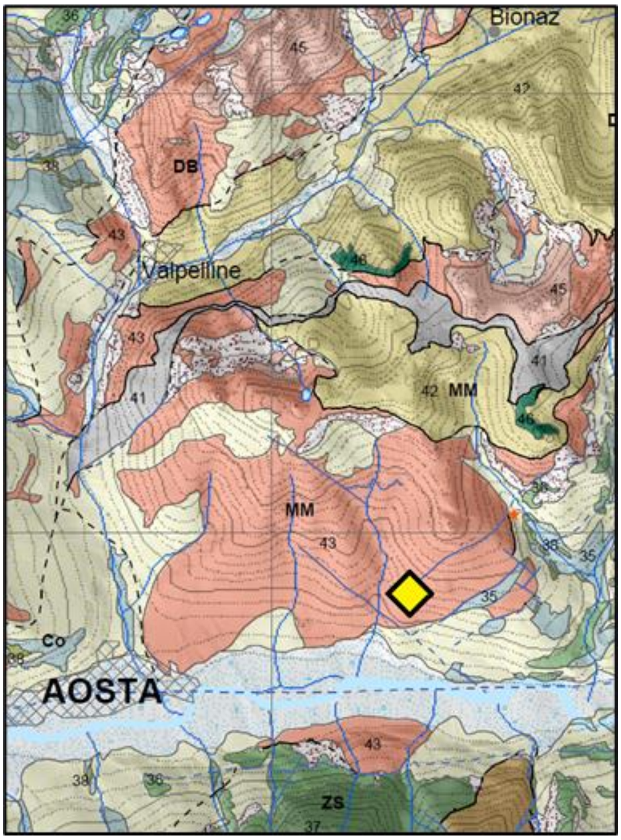

Figure 14: Extract from the Geotectonic Map of the Aosta Valley (modified by De Giusti et al., 2004). The Quart Castle is identified with the yellow rhombus. The unit of the Valpelline Series include n.42 which identifies the kinzigites (light brown) togheter with n.43 orthoterivates in pink; the eclogitic units of the Zermatt-Saas zone (ZS) are indicated with the n.37.

In all the analyzed samples there are often single feldspar crystals, which together with the white mica and quartz crystals probably derive from the dismantling of more or less metamorphosed continental crust units. The potassium feldspar inclusions, in particular, could derive from the dismantling of orthogneiss, such as those of the Gran Paradiso massif outcropping in the Valsavaranche Valley, or of granite, probably deriving from the erosion of the granite of Mont Blanc massif. The lithic clasts with a granite composition found in some sections, especially those sampled in the Quart Castle, could also derive from this last massif.

Plagioclases with a labradorite composition can refer to basic rocks or to units of high metamorphic grade. Also, in this case there is a congruence between the data found from the analyses of the Quart Castle binder and the location of the castle. In the unit of the Valpelline Series in fact high temperature basic masses occur.

A lithology frequently present in the samples from both castles are the graphitic-schists, which appear to be present in greater quantities and in greater dimensions in the mortars of Châtel Argent Castle and in smaller quantities and of much smaller dimensions in those of the Quart Castle. These lithic fragments most likely derive from the dismantling of graphitic-schists belonging to the units of the Houillère Zone out cropping just upstream of the site where the Châtel Argent Castle is located (**Figure 15**). In this case, also the petrographic analysis of the aggregate is consistent with the regional geology of the areas surrounding the buildings studied. The calcschist are probably referable to the Mesozoic covers of oceanic crust of the Piemonte Zone (**Figure 15**).

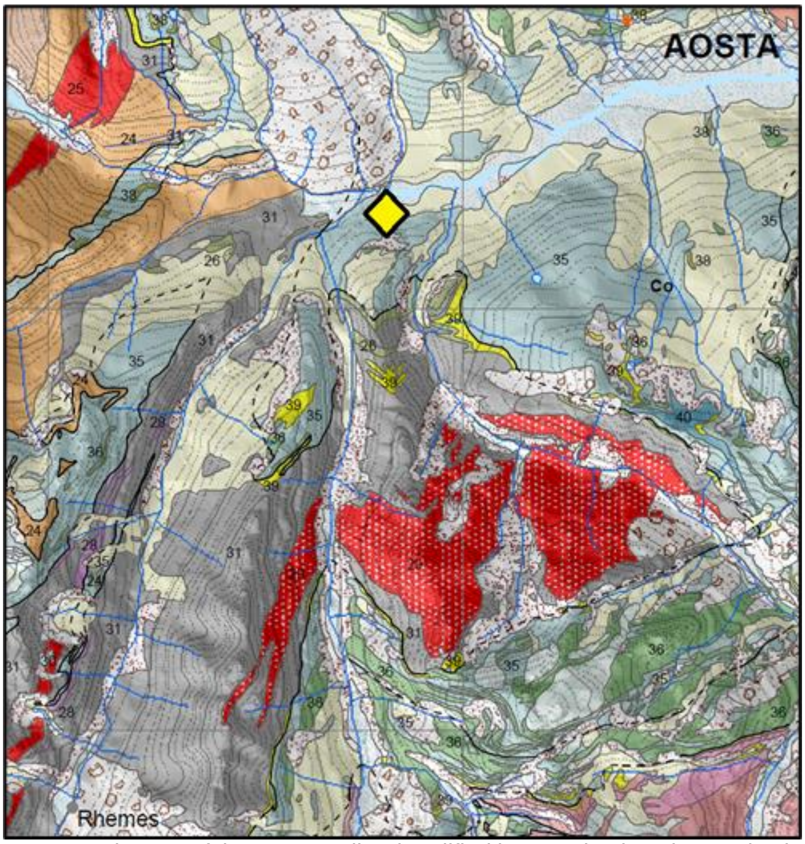

Figure 15: Extract from Geotectonic Map of the Aosta Valley (modified by De Giusti et al., 2004). The Châtel Argent Castle is identified with the yellow rhombus. The n. 31 identifies the Briaçonnais Unit of Permo-Carboniferous age containing graphitic-schists, while the n. 35 identifies the units of origin of calcschists.

7. Conclusions

On the basis of the petrographic and mineralogical analyses, it can be concluded that the aggregate used in medieval times to make the bedding mortars and plasters used in the two historic buildings can be classified as river sand, coming from alluvial deposits of the Dora Baltea River located in the immediate proximity to the sites where the two castles stand.

Only in limited quantities were used materials from crushed rocks, such as the inclusions of calcite from vein observed in numerous samples analyzed or, in the only case of the ACK17 sample from Châtel Argent Castle, of artificial materials with pozzolanic behavior, such as the inclusions of cocciopesto and melting slag.

The possible finding of raw materials to be used for potential restoration works must therefore be sought in the vicinity of historical sites. In particular, in the case of the Quart Castle:

- In fluvial sands located at the confluence of the Buthier Stream in the Dora Baltea River, which are characterized by rock fragments coming from the Valpelline Series and calcschist from the Piemonte Zone.

In the case of the Châtel Argent Castle:

- In fluvial sands located just downstream of the confluence of the Dora di Rhemes and Savara streams into the Dora Baltea River, rich in clasts deriving from the dismantling of the units of the External Briançonnais Zone and of the calcschists of the Piemonte Zone.

In conclusion, it can be stated that the petrographic observation accompanied by an in-depth analysis using scanning electron microscopy and attached electron microprobe has resulted in an analytical approach useful for the characterization of historical mortars, defining the basins of origin of the raw materials used for the realization of the same, and therefore guiding the choice of the best materials for future restoration operations.

Acknowledgments

The research was supported by the University of Torino (ex 60% funds). It was carried out in the frame of GeoDIVE Project (M. Giardino coord.), funded by Compagnia di San Paolo Foundation and University of Torino. Two Anonymous reviewers and editor are acknowledged for their constructive comments and remarks, which improved the manuscript. A special thanks to Dario Vaudan for the XRPD analyses.

References

Appolonia, L., De Gattis, G., Fioravanti, P., Pizzi, L., Vaudan, D., Zidda, G., Bedini, E., Bertone, A., Cortellazzo, M., Hurni, J. P., Lupo, M., Orcel, C., Tercier, J., 2006. Il Castello di Quart. Bollettino Soprintendenza per i beni e le attività culturali della Valle d'Aosta n.2. ©RAVA, pp. 71-122. https://gestionewww.regione.vda.it/cultura/pubblicazioni/bollettino/n_2/default_i.aspx.

Appolonia, L., Vaudan, D., Glarey, A., 2010. Il castello di Châtel-Argent a Villeneuve: il contributo allo studio dei materiali in relazione alla fornace da calce. Bollettino Soprintendenza per i beni e le attività culturali della Valle d'Aosta n.6. ©RAVA, pp. 108-111. https://gestionewww.regione.vda.it/cultura/pubblicazioni/bollettino/n_6/default_i.aspx

Arizzi, A., Cultrone, G., 2012. The difference in behaviour between calcitic and dolomitic lime mortars set under dry conditions: The relationship between textural and physical–mechanical properties. Cement and Concrete Research. 42, 818-826. https://doi.org/10.1016/j.cemconres.2012.03.008.

Beltrando, M., Compagnoni, R., Lombardo, B., 2010. (Ultra) High-pressure metamorphism and orogenesis: an Alpine perspective. Gondwana Research. 18, 147-166. https://doi.org/10.1016/j.gr.2010.01.009

Biehl, L., Landgrebe, D. A., 2002. MultiSpec: a tool for multispectral-hyperspectral image data analysis. Computer & Geosciences. 38, 1153-1159. https://doi.org/10.1016/S0098-3004(02)00033-X

Cantù, M., Giacometti, F., Landi, A. G., Riccardi, M. P., Tarantino, S. C., Grimoldi, A., 2015. Characterization of XVIIIth century earthen mortars from Cremona (Northern Italy): Insights on a manufacturing tradition. Materials Characterization. 103, 81-89. https://doi.org/10.1016/j.matchar.2015.03.018

Cosano, D., Esquivel, D., Jimenez-Sanchidrian, C., Ruiz, J.R., 2021. Analysis of mortars from the castle keep in Priego de Cordoba (Spain). Vibrational Spectroscopy, 112, 103184.

Carò, F., Riccardi, M.P., Mazzilli Savini, M.T., 2008. Characterization of plasters and mortars as a tool in archaeological studies: the case of Lardirago Castle in Pavia, Northern Italy, Archaeometry 50, 1, 85–100.

Dal Piaz, G. V., 1999. The Austroalpine–Piedmont nappe stack and the puzzle of Alpine Tethys. Memorie di Scienze Geologiche. 51(1), 155-176.

Dal Piaz, G. V., Hunziker, J. C., Martinotti, G., 1972. La Zona Sesia Lanzo e l'evoluzione tettono-metamorfica delle Alpi nordoccidentali interne. Memorie Società Geologica Italiana. 11, 433-466.

De Gattis, G., Cortellazzo, M., 2008. Indagini archeologiche al sito fortificato di Châtel-Argent (Villeneuve) tra tarda antichità e Medioevo. Bollettino Soprintendenza per i beni e le attività culturali della Valle d'Aosta n.4. ©RAVA, pp. 203-211. https://www.regione.vda.it/cultura/pubblicazioni/bollettino/n_4/default_i.aspx

De Giusti, F., Dal Piaz, G. V., Massironi, M., Schiavo, A., 2004. Carta geotettonica della Valle d'Aosta. Memorie di Scienze Geologiche. 55, 129-149.

Elsen, J., 2006. Microscopy of historic mortars - a review. Cement and Concrete Research. 36(8), 1416-1424. https://doi.org/10.1016/j.cemconres.2005.12.006

Elter, G., Elter, P., 1965. Carta geologica della regione del Piccolo S. Bernardo (versante italiano): note illustrative. Memorie Istituto Geologico Mineralogico Università di Padova. Societa Cooperativa Tipografica, Padova. 25, 1-53.

Ernst, W. G., Dal Piaz, G. V., 1978. Mineral parageneses of eclogitic rocks and related mafic schists of the Piemonte ophiolite nappe, Breuil – St. Jacques area, Italian Western Alps. American Mineralogist, 63(7-8), 621-640.

Lezzerini, M., Ramacciotti, M., Cantini, F., Fatighenti, B., Antonelli, F., Pecchioni, E., Fratini, F., Cantisani, E., Giamello, M., 2017. Archaeometric study of natural hydraulic mortars: the case of the Late Roman Villa dell'Oratorio (Florence, Italy). Archaeological and Anthropological Sciences. 9, 603-615. https://doi.org/10.1007/s12520-016-0404-2

Lezzerini, M., Raneri, S., Pagnotta, S., Columbu, S., Gallello, G., 2018. Archaeometric study of mortars from the Pisa's Cathedral Square (Italy). Measurement. 126, 322-331. https://doi.org/10.1016/j.measurement.2018.05.057

Loprieno, A., Bousquet, R., Bucher, S., Ceriani, S., Dalla Torre, F. H., Fugenschuh, B., Schmid, S. M., 2011. The Valais units in Savoy (France): a key area for understanding the palaeogeography and the tectonic evolution of the Western Alps. International Journal of Earth Sciences. 100, 963–92. https://doi.org/10.1007/s00531-010-0595-1

Malusà, G., Polino, R., Martin, S., 2005. The Gran San Bernardo nappe in the Aosta Valley (Western Alps): a composite stack of distinct continental crust units. Bulletin de la Société Géologique de France. 176(5), 417-431. https://doi.org/10.2113/176.5.417

Mannoni, T., 1988. Ricerche sulle malte genovesi alla «porcellana», Atti del Convegno di Studi «Le Scienze, le Istituzioni, gli Operatori alla soglia degli anni '90», Bressanone, 137-142.

Mariani, E., 1976. I leganti aerei e idraulici. Ed. Ambrosiana, Milano.

Martinotti, G., Giordan, D., Giardino, M., Ratto, S., 2011. Controlling factors for deep-seated gravitational slope deformation (DSGSD) in the Aosta Valley (NW Alps, Italy). Jaboyedoff, M. (ed.) Slope Tectonics. Geological Society London Special Publications. 351(1), 113–131. http://dx.doi.org/10.1144/SP351.6

Miriello, D., Barca, D., Bloise, A., Ciarallo, A., Crisci, G. M., De Rose, T., Gattuso, C., Gazineo, F., La Russa, M. F., 2010. Characterisation of archaeological mortars from Pompeii (Campania, Italy) and identification of construction phases by compositional data analysis. Journal of Archaeological Science. 37(9), 2207-2223. https://doi.org/10.1016/j.jas.2010.03.019

Morimoto, N., 1988. Nomenclature of Pyroxenes. Mineralogy and Petrology. 39, 55–76. https://doi.org/10.1007/BF01226262

Moropoulou, A., Bakolas, A., Bisbikou, K., 2000. Investigation of the technology of historic mortars. Journal of Cultural Heritage. 1, 45-58. https://doi.org/10.1016/S1296-2074(99)00118-1

NORMA UNI 10924, 2001. Malte per elementi costruttivi e decorativi: classificazione e terminologia. Ed UNI (Ente Nazionale Italiano Unificazione) Milano.

Pecchioni, E., Fratini, F., Cantisani, E., 2018. Le malte antiche e moderne tra tradizione ed innovazione, second ed. Pàtron, Bologna.

Petrakakis, K., Dietrich, H., 1985. MINSORT: a program for the processing and archivation of microprobe analyses of silicate and oxide minerals. Neues Jahrbuch für Mineralogie, Monatshefte. 74(8), 379-384.

Polino, R., Bonetto, F., Carraro, F., Gianotti, F., Gouffon, Y., Malusà, M.G., Martin, S., Perello, P., Schiavo, A., 2015. Note Illustrative della Carta Geologica d'Italia alla scala 1:50.000 - Foglio 090AOSTA. ISPRA, Roma.

Ponce-Antón G., Zuluaga M.C., Ortega, L.A., Mauleon, J.A., 2020. Petrographic and Chemical–Mineralogical Characterization of Mortars from the Cistern at Amaiur Castle (Navarre, Spain). Minerals, 10, 311.

Ponce-Antón, G., Arizzi, A., Cultrone, G., Zuluaga, M.C.I., Ortega, L.A., Mauleon, J.A., 2021. Investigating the manufacturing technology and durability of lime mortars from Amaiur Castle (Navarre, Spain): A chemical–mineralogical and physical study. Construction and Building Materials 299.

Rampazzi, L., Colombini, M., Conti, C., Corti, C., Lluveras-Tenorio, A., Sansonetti, A., Zanaboni, M., 2016. Technology of Medieval Mortars: An Investigation into the Use of Organic Additives. Archaeometry, Wiley. 58, 115-130. https://doi.org/10.1111/arcm.12155

Rapp, G., 2009. Archaeomineralogy, second ed. Natural Sciences in Archaeology, Springer-Verlag Berlin Heidelberg. doi:10.1007/978-3-540-78594-1.

Riccardi, M. P., Lezzerini, M., Carò, F., Franzini, M., Messiga, B., 2007. Microtextural and microchemical studies of hydraulic ancient mortars: Two analytical approaches to understand pre-industrial technology process. Journal of Cultural heritage. 8, 350-360. https://doi.org/10.1016/j.culher.2007.04.005

Scherer, G.W., 1990. Theory of drying. Journal of the American Ceramic Society. 73(1) 3-14. https://doi.org/10.1111/j.1151-2916.1990.tb05082.x

Schiele, E., Berens, L.W., 1976. La Calce. Calcare, calce viva, idrato di calcio. Ed. Tecniche ET, Milano.

Whitney, D.L., Evans, B.W., 2010. Abbreviations for Names of Rock-Forming Minerals. American Mineralogist. 95, 185-187. http://dx.doi.org/10.2138/am.2010.3371

Pyroxene

SAMPLE	*ACK04*		*ACK12*	*ADY04*				*ADY17*				
SiO2	53,16	52,34	52,20	47,94	46,53	46,47	47,94	51,83	50,20	51,94	52,03	50,86
Al2O3	4,23	3,53	6,72	9,71	11,05	11,00	10,14	2,08	2,70	1,94	1,89	2,97
FeO	1,67	9,78	14,71	19,28	19,84	19,92	17,29	13,39	15,19	12,77	13,46	14,25
MgO	15,89	13,58	13,39	10,39	9,93	9,90	11,59	10,86	11,20	11,15	11,21	11,34
CaO	25,06	20,78	12,23	11,35	11,08	11,16	11,62	21,46	20,34	21,85	21,06	20,23
Na2O	0,00	0,00	0,76	1,33	1,56	1,54	1,42	0,39	0,37	0,35	0,34	0,35
	******	******	******	******	******	******	******	******	******	******	******	******
Total	100,01	100,01	100,01	100,00	99,99	99,99	100,00	100,01	100,00	100,00	99,99	100,00
Si	1,925	1,943	1,929	1,814	1,758	1,757	1,795	1,967	1,907	1,967	1,973	1,928
Al IV	0,075	0,057	0,071	0,186	0,242	0,243	0,205	0,033	0,060	0,033	0,027	0,066
Fe 3+	0,000	0,000	0,000	0,000	0,000	0,000	0,000	0,000	0,032	0,000	0,000	0,006
Al VI	0,105	0,098	0,221	0,246	0,251	0,247	0,242	0,060	0,060	0,054	0,057	0,066
Fe 3+	0,000	0,000	0,000	0,037	0,105	0,109	0,066	0,002	0,060	0,005	0,000	0,032
Fe 2+	0,050	0,260	0,297	0,354	0,311	0,311	0,293	0,382	0,335	0,366	0,380	0,354
Mg	0,845	0,643	0,482	0,362	0,333	0,333	0,399	0,556	0,545	0,576	0,563	0,548
Fe 2+	0,001	0,044	0,158	0,219	0,211	0,210	0,183	0,040	0,055	0,034	0,047	0,060
Mg	0,012	0,109	0,256	0,224	0,226	0,225	0,248	0,059	0,090	0,054	0,070	0,093
Ca	0,972	0,827	0,484	0,460	0,449	0,452	0,466	0,872	0,828	0,887	0,855	0,822
Na	0,000	0,000	0,054	0,098	0,114	0,113	0,103	0,029	0,027	0,026	0,025	0,026
T	2,000	2,000	2,000	2,000	2,000	2,000	2,000	2,000	2,000	2,000	2,000	2,000
M(1)	1,000	1,000	1,000	1,000	1,000	1,000	1,000	1,000	1,000	1,000	1,000	1,000
M(2)	0,985	0,980	0,952	1,000	1,000	1,000	1,000	1,000	1,000	1,000	0,998	1,000
Xmg	0,944	0,712	0,619	0,506	0,517	0,517	0,576	0,592	0,619	0,612	0,598	0,607

Table S1: Representative microprobe analyses of pyroxenes of Châtel Argent Castle (ACK04 and ACK12) and Quart Castle (ADY04 and ADY17). The chemical composition of minerals is expressed as weight% oxides. The structural formulae, reported as number of cations per formula unit (a.p.f.u.), were recalculated on the basis of 6 oxygens. T= Tetrahedral site, M(1)= Octahedral site, M(2)= distorted 6- or 8-fold site, Xmg= Mg/(Mg+Fe^{2+}+Fe^{3+}).

Amphibole

SAMPLE	*ACK10*	*ADY04*		*ADY10*								
SiO2	52,40	56,86	56,25	56,11	55,73	55,96	51,68	53,70	52,72	46,67	46,54	46,73
Al2O3	5,62	0,62	1,76	1,63	1,97	1,80	3,97	3,58	4,81	9,14	9,88	9,91
FeO	15,13	10,11	11,21	10,47	11,79	11,03	15,49	15,32	14,75	19,81	18,48	18,45
MgO	13,26	17,97	16,44	17,58	16,54	17,11	14,21	13,90	13,81	10,47	9,91	10,04
CaO	10,25	11,93	11,56	11,35	11,07	11,11	11,57	9,79	10,19	10,54	11,17	11,19
Na2O	1,32	0,51	0,78	0,87	0,89	0,99	1,05	1,72	1,72	1,20	1,71	1,41
K2O	0,02	0,00	0,00	0,00	0,00	0,00	0,04	0,00	0,00	0,18	0,31	0,27
	******	******	******	******	******	******	******	******	******	******	******	******
Total	98,00	98,00	98,01	98,00	98,00	98,00	98,02	98,00	98,00	98,01	98,00	98,00
Si	7,487	8,000	7,955	7,914	7,903	7,911	7,424	7,653	7,505	6,781	6,843	6,842
Al IV	0,513	0,000	0,045	0,086	0,097	0,089	0,576	0,347	0,495	1,219	1,157	1,158
Al VI	0,432	0,103	0,249	0,185	0,232	0,211	0,096	0,254	0,313	0,347	0,555	0,551
Fe 3+	0,444	0,036	0,000	0,000	0,000	0,000	0,620	0,567	0,599	1,176	0,536	0,644
Mg	2,824	3,770	3,465	3,697	3,497	3,606	3,044	2,952	2,931	2,267	2,172	2,190
Fe 2+	1,300	1,091	1,286	1,118	1,271	1,183	1,240	1,227	1,157	1,210	1,737	1,615
Fe 2+	0,065	0,063	0,040	0,116	0,128	0,121	0,000	0,031	0,000	0,021	0,000	0,000
Ca	1,569	1,798	1,751	1,715	1,682	1,683	1,780	1,495	1,555	1,642	1,760	1,756
Na	0,366	0,139	0,209	0,169	0,190	0,196	0,220	0,474	0,445	0,337	0,240	0,244
Na	0,000	0,000	0,006	0,070	0,055	0,075	0,072	0,000	0,028	0,000	0,246	0,156
K	0,004	0,000	0,000	0,000	0,000	0,000	0,007	0,000	0,000	0,033	0,059	0,051
Xmg	0,674	0,766	0,723	0,750	0,714	0,735	0,711	0,701	0,717	0,648	0,556	0,576
Fe2O3	4,214	0,344	0,000	0,000	0,000	0,000	5,855	5,396	5,701	10,970	4,944	5,965
FeO	11,648	10,010	11,440	10,680	12,030	11,250	10,531	10,775	9,920	10,339	14,411	13,453

Amphibole								
SAMPLE	*ADY10*	*ADY17*						
SiO2	46,75	48,83	50,70	49,74	43,25	43,23	43,21	42,93
Al2O3	10,28	9,25	6,86	9,19	13,22	13,18	13,35	13,06
FeO	18,18	16,57	15,67	16,12	17,98	18,17	17,93	18,70
MgO	9,83	11,52	13,06	11,44	9,03	8,87	8,85	8,71
CaO	11,13	9,00	9,51	8,53	11,56	11,51	11,61	11,53
Na2O	1,46	2,72	2,20	2,98	1,43	1,44	1,45	1,50
K2O	0,37	0,11	0,00	0,00	1,53	1,60	1,60	1,57
	******	******	******	******	******	******	******	******
Total	98,00	98,00	98,00	98,00	98,00	98,00	98,00	98,00
Si	6,850	6,995	7,214	7,098	6,438	6,446	6,447	6,419
Al IV	1,150	1,005	0,786	0,902	1,562	1,554	1,553	1,581
Al VI	0,625	0,556	0,365	0,644	0,758	0,763	0,794	0,720
Fe 3+	0,545	0,912	0,915	0,827	0,411	0,391	0,323	0,432
Mg	2,147	2,459	2,771	2,433	2,003	1,972	1,968	1,942
Fe 2+	1,683	1,073	0,950	1,096	1,828	1,874	1,915	1,906
Fe 2+	0,000	0,000	0,000	0,000	0,000	0,000	0,000	0,000
Ca	1,748	1,381	1,449	1,303	1,845	1,840	1,856	1,848
Na	0,252	0,619	0,551	0,697	0,155	0,160	0,144	0,152
Na	0,163	0,137	0,057	0,128	0,258	0,256	0,276	0,282
K	0,070	0,020	0,000	0,000	0,290	0,304	0,304	0,299
Xmg	0,561	0,700	0,745	0,689	0,523	0,513	0,507	0,505
Fe2O3	5,044	8,632	8,717	7,864	3,746	3,560	2,934	3,918
FeO	14,011	9,143	8,147	9,374	14,979	15,337	15,660	15,555

Table S2: Representative microprobe analyses of amphiboles of Châtel Argent Castle (ACK10) and Quart Castle (ADY04, ADY10 and ADY17). The chemical composition of minerals is expressed as weight% oxides. The structural formulae, reported as number of cations per formula unit (a.p.f.u.), were recalculated on the basis of 23 oxygens. Xmg= Mg/(Mg+Fe^{2+}+Fe^{3+}).

Feldspar

SAMPLE	*ACK04*				*ACK10*						*ACK12*	
SiO2	69,34	69,17	68,70	69,10	69,18	69,31	69,44	69,19	68,96	69,30	68,91	69,07
Al2O3	19,45	19,43	19,62	19,56	19,43	19,28	19,39	19,43	19,52	19,33	19,62	19,40
CaO	0,00	0,00	0,30	0,00	0,00	0,00	0,00	0,00	0,23	0,00	0,20	0,00
Na2O	11,09	11,40	11,38	11,34	11,39	11,41	11,17	11,38	11,29	11,37	11,28	11,53
K2O	0,12	0,00	0,00	0,00	0,00	0,00	0,00	0,00	0,00	0,00	0,00	0,00
	******	******	******	******	******	******	******	******	******	******	******	******
Total	100,00	100,00	100,00	100,00	100,00	100,00	100,00	100,00	100,00	100,00	100,01	100,00
Si	3,017	3,012	2,996	3,008	3,012	3,017	3,019	3,012	3,004	3,016	3,002	3,009
Al	0,997	0,997	1,008	1,004	0,997	0,989	0,994	0,997	1,002	0,992	1,007	0,996
Ca	0,000	0,000	0,014	0,000	0,000	0,000	0,000	0,000	0,011	0,000	0,009	0,000
Na	0,935	0,962	0,963	0,957	0,961	0,963	0,942	0,961	0,954	0,960	0,953	0,974
K	0,007	0,000	0,000	0,000	0,000	0,000	0,000	0,000	0,000	0,000	0,000	0,000
Z	4,014	4,009	4,004	4,012	4,009	4,007	4,013	4,009	4,007	4,008	4,009	4,006
X	0,942	0,962	0,977	0,957	0,961	0,963	0,942	0,961	0,964	0,960	0,962	0,974
An	0,000	0,000	0,014	0,000	0,000	0,000	0,000	0,000	0,011	0,000	0,010	0,000
Ab	0,993	1,000	0,986	1,000	1,000	1,000	1,000	1,000	0,989	1,000	0,990	1,000
Or	0,007	0,000	0,000	0,000	0,000	0,000	0,000	0,000	0,000	0,000	0,000	0,000

Feldspar

SAMPLE	ACK12						ACK17	ADY04				
SiO2	68,76	69,20	69,35	69,31	69,22	69,35	69,20	66,62	68,92	69,41	68,56	68,98
Al2O3	19,78	19,45	19,40	19,37	19,42	19,43	19,24	23,42	19,42	19,36	19,81	19,59
CaO	0,00	0,00	0,00	0,00	0,00	0,00	0,00	0,77	0,15	0,00	0,11	0,00
Na2O	11,47	11,35	11,26	11,32	11,36	11,23	11,54	9,19	11,51	11,23	11,51	11,44
K2O	0,00	0,00	0,00	0,00	0,00	0,00	0,02	0,00	0,00	0,00	0,00	0,00
	******	******	******	******	******	******	******	******	******	******	******	******
Total	100,01	100,00	100,01	100,00	100,00	100,01	100,00	100,00	100,00	100,00	99,99	100,01
Si	2,996	3,012	3,017	3,016	3,013	3,016	3,015	2,891	3,005	3,019	2,990	3,004
Al	1,016	0,998	0,995	0,993	0,996	0,996	0,988	1,198	0,998	0,992	1,018	1,006
Ca	0,000	0,000	0,000	0,000	0,000	0,000	0,000	0,036	0,007	0,000	0,005	0,000
Na	0,969	0,958	0,950	0,955	0,959	0,947	0,975	0,773	0,973	0,947	0,973	0,966
K	0,000	0,000	0,000	0,000	0,000	0,000	0,001	0,000	0,000	0,000	0,000	0,000
Z	4,012	4,010	4,011	4,010	4,009	4,012	4,003	4,088	4,003	4,011	4,009	4,010
X	0,969	0,958	0,950	0,955	0,959	0,947	0,976	0,809	0,980	0,947	0,978	0,966
An	0,000	0,000	0,000	0,000	0,000	0,000	0,000	0,044	0,007	0,000	0,005	0,000
Ab	1,000	1,000	1,000	1,000	1,000	1,000	0,999	0,956	0,993	1,000	0,995	1,000
Or	0,000	0,000	0,000	0,000	0,000	0,000	0,001	0,000	0,000	0,000	0,000	0,000

Feldspar

SAMPLE	ADY04	ADY10					ADY17					
SiO2	68,96	68,89	68,76	69,42	68,70	68,47	55,88	56,77	69,12	68,94	53,46	54,60
Al2O3	19,41	19,54	19,51	19,36	19,77	20,15	25,22	24,83	19,24	18,91	29,98	29,12
CaO	0,00	0,00	0,35	0,00	0,53	0,62	12,64	12,19	0,00	0,54	12,18	11,17
Na2O	11,63	11,57	11,39	11,21	11,00	10,77	6,26	6,21	11,64	11,61	4,38	5,11
K2O	0,00	0,00	0,00	0,00	0,00	0,00	0,00	0,00	0,00	0,00	0,00	0,00
	******	******	******	******	******	******	******	******	******	******	******	******
Total	100,00	100,00	100,01	99,99	100,00	100,01	100,00	100,00	100,00	100,00	100,00	100,00
Si	3,006	3,003	2,999	3,019	2,994	2,982	2,541	2,573	3,013	3,011	2,413	2,459
Al	0,997	1,004	1,003	0,992	1,015	1,034	1,351	1,326	0,988	0,974	1,595	1,546
Ca	0,000	0,000	0,016	0,000	0,025	0,029	0,616	0,592	0,000	0,025	0,589	0,539
Na	0,983	0,978	0,963	0,945	0,929	0,910	0,552	0,546	0,984	0,983	0,383	0,446
K	0,000	0,000	0,000	0,000	0,000	0,000	0,000	0,000	0,000	0,000	0,000	0,000
Z	4,004	4,007	4,002	4,012	4,009	4,017	3,892	3,899	4,001	3,985	4,008	4,005
X	0,983	0,978	0,980	0,945	0,954	0,938	1,168	1,138	0,984	1,009	0,972	0,985
An	0,000	0,000	0,017	0,000	0,026	0,031	0,527	0,520	0,000	0,025	0,606	0,547
ab	1,000	1,000	0,983	1,000	0,974	0,969	0,473	0,480	1,000	0,975	0,394	0,453
Or	0,000	0,000	0,000	0,000	0,000	0,000	0,000	0,000	0,000	0,000	0,000	0,000

Feldspar											
SAMPLE	*ACK10*		*ACK12*				*ADY04*	*ADY10*			
SiO2	65,69	65,92	65,92	66,08	65,92	65,90	65,97	66,40	66,07	66,08	65,90
Al2O3	18,47	18,57	18,42	18,51	18,44	18,31	18,57	18,28	18,52	18,43	18,59
CaO	0,00	0,00	0,00	0,00	0,00	0,00	0,00	0,00	0,00	0,00	0,00
Na2O	0,73	0,46	0,27	0,59	0,49	0,60	0,00	0,35	0,30	0,32	0,50
K2O	15,11	15,05	15,39	14,82	15,15	15,19	15,46	14,97	15,10	15,17	15,01
	******	******	******	******	******	******	******	******	******	******	******
Total	100,00	100,00	100,00	100,00	100,00	100,00	100,00	100,00	99,99	100,00	100,00
Si	3,014	3,018	3,022	3,022	3,021	3,022	3,022	3,035	3,024	3,026	3,017
Al	0,999	1,002	0,995	0,998	0,996	0,990	1,003	0,985	0,999	0,994	1,003
Ca	0,000	0,000	0,000	0,000	0,000	0,000	0,000	0,000	0,000	0,000	0,000
Na	0,065	0,041	0,024	0,052	0,044	0,053	0,000	0,031	0,027	0,028	0,044
K	0,884	0,879	0,900	0,865	0,886	0,889	0,904	0,873	0,882	0,886	0,877
Z	4,012	4,021	4,018	4,020	4,017	4,012	4,025	4,020	4,023	4,020	4,021
X	0,949	0,920	0,924	0,917	0,929	0,942	0,904	0,904	0,908	0,914	0,921
An	0,000	0,000	0,000	0,000	0,000	0,000	0,000	0,000	0,000	0,000	0,000
Ab	0,068	0,044	0,026	0,057	0,047	0,057	0,000	0,034	0,029	0,031	0,048
Or	0,932	0,956	0,974	0,943	0,953	0,943	1,000	0,966	0,971	0,969	0,952

Table S3: Representative microprobe analyses of feldspars of Châtel Argent Castle (ACK04, ACK10, ACK12 and ACK17) and Quart Castle (ADY04, ADY10 and ADY17). The chemical composition of minerals is expressed as weight% oxides. The structural formulae, reported as number of cations per formula unit (a.p.f.u.), were recalculated on the basis of 8 oxygens. Z= Tetrahedral site, X= large, irregularly coordinated site. An= Anorthite Ab= Albite, Or= Orthoclase (Mineral abbreviations according to Whitney and Evans, 2010).

Dioctahedral micas

SAMPLE	*ACK04*					*ACK10*						
SiO2	48,19	47,30	55,33	54,26	53,82	51,45	53,81	51,40	51,02	49,95	52,04	48,21
Al2O3	27,41	21,79	24,13	26,24	26,65	27,36	26,86	27,42	27,48	31,04	27,92	34,65
FeO	3,08	6,23	0,00	0,00	0,00	2,99	1,03	2,94	3,20	1,84	2,54	0,88
MgO	1,02	4,88	5,29	4,87	4,47	2,82	4,04	3,14	3,10	2,20	2,96	1,23
CaO	0,00	1,02	0,39	0,00	0,00	0,47	0,00	0,00	0,00	0,00	0,00	0,00
Na2O	4,13	9,52	0,32	0,00	0,00	0,33	0,00	0,00	0,00	0,48	0,00	0,65
K2O	11,17	4,27	9,54	9,62	10,06	9,58	9,27	10,11	10,20	9,49	9,54	9,38
	******	******	******	******	******	******	******	******	******	******	******	******
Total	95,00	95,00	95,00	95,00	95,00	95,00	95,00	95,00	95,00	95,00	95,00	95,00
Si	6,623	6,559	7,245	7,093	7,055	6,864	7,051	6,860	6,826	6,616	6,894	6,356
Al IV	1,377	1,441	0,755	0,907	0,945	1,136	0,949	1,140	1,174	1,384	1,106	1,644
Al VI	3,064	2,120	2,968	3,135	3,171	3,165	3,199	3,172	3,160	3,460	3,254	3,741
Fe	0,354	0,723	0,000	0,000	0,000	0,334	0,112	0,328	0,358	0,204	0,281	0,097
Mg	0,208	1,010	1,033	0,950	0,874	0,561	0,789	0,624	0,618	0,435	0,585	0,243
Ca	0,000	0,151	0,055	0,000	0,000	0,068	0,000	0,000	0,000	0,000	0,000	0,000
Na	1,101	2,560	0,082	0,000	0,000	0,086	0,000	0,000	0,000	0,122	0,000	0,165
K	1,959	0,755	1,593	1,605	1,682	1,630	1,550	1,721	1,742	1,604	1,612	1,577
Z	8,000	8,000	8,000	8,000	8,000	8,000	8,000	8,000	8,000	8,000	8,000	8,000
Y	3,626	3,852	4,001	4,084	4,046	4,060	4,100	4,124	4,136	4,099	4,120	4,081
X	3,060	3,466	1,730	1,605	1,682	1,784	1,550	1,721	1,742	1,725	1,612	1,742
Xmg	0,371	0,583	1,000	1,000	1,000	0,627	0,875	0,656	0,633	0,681	0,676	0,714
Ms	0,640	0,218	0,921	1,000	1,000	0,914	1,000	1,000	1,000	0,929	1,000	0,905
pg	0,360	0,739	0,047	0,000	0,000	0,048	0,000	0,000	0,000	0,071	0,000	0,095
ma	0,000	0,044	0,032	0,000	0,000	0,038	0,000	0,000	0,000	0,000	0,000	0,000

Dioctahedral micas

SAMPLE	*ACK10*	*ACK12*										*ACK17*
SiO2	49,63	51,09	53,76	49,36	52,90	53,30	47,41	47,60	46,93	53,03	54,21	52,33
Al2O3	28,09	29,84	25,46	32,95	27,06	25,52	39,74	39,42	38,31	27,68	26,23	25,57
FeO	5,09	0,47	1,07	0,38	0,73	1,14	0,00	0,30	0,00	0,00	1,65	3,48
MgO	2,07	3,39	4,83	2,18	4,21	4,76	0,00	0,00	0,52	4,16	4,05	2,91
CaO	0,00	0,00	0,00	0,00	0,00	0,00	0,39	0,00	1,81	0,00	0,00	1,49
Na2O	0,67	0,62	0,00	0,90	0,53	0,30	6,68	7,43	7,16	0,44	0,00	3,36
K2O	9,44	9,60	9,88	9,22	9,58	9,98	0,78	0,25	0,27	9,69	8,86	5,87
	******	******	******	******	******	******	******	******	******	******	******	
Total	95,00	95,00	95,00	95,00	95,00	95,00	95,00	95,00	95,00	95,00	95,00	95,00
Si	6,701	6,727	7,086	6,490	6,963	7,046	6,048	6,071	6,024	6,952	7,105	6,947
Al IV	1,299	1,273	0,914	1,510	1,037	0,954	1,952	1,929	1,976	1,048	0,895	1,053
Al VI	3,171	3,357	3,040	3,597	3,160	3,022	4,022	3,996	3,818	3,230	3,156	2,949
Fe	0,575	0,051	0,118	0,042	0,081	0,126	0,000	0,032	0,000	0,000	0,181	0,386
Mg	0,417	0,666	0,948	0,428	0,826	0,938	0,000	0,000	0,100	0,813	0,791	0,575
Ca	0,000	0,000	0,000	0,000	0,000	0,000	0,053	0,000	0,248	0,000	0,000	0,212
Na	0,174	0,158	0,000	0,230	0,136	0,078	1,652	1,837	1,783	0,111	0,000	0,866
K	1,627	1,612	1,661	1,547	1,608	1,682	0,127	0,040	0,044	1,621	1,482	0,994
Z	8,000	8,000	8,000	8,000	8,000	8,000	8,000	8,000	8,000	8,000	8,000	8,000
Y	4,163	4,074	4,107	4,067	4,067	4,086	4,022	4,028	3,918	4,043	4,128	3,910
X	1,801	1,769	1,661	1,777	1,744	1,760	1,832	1,877	2,074	1,732	1,482	2,072
Xmg	0,420	0,929	0,889	0,911	0,911	0,882	0,000	0,000	1,000	1,000	0,814	0,598
Ms	0,903	0,911	1,000	0,871	0,922	0,956	0,069	0,021	0,021	0,936	1,000	0,480
Pg	0,097	0,089	0,000	0,129	0,078	0,044	0,902	0,979	0,859	0,064	0,000	0,418
Mrg	0,000	0,000	0,000	0,000	0,000	0,000	0,029	0,000	0,120	0,000	0,000	0,102

Dioctahedral micas

SAMPLE	*ADY04*											
SiO2	51,32	50,84	50,96	49,04	53,99	50,55	52,54	51,00	48,83	48,43	49,37	47,45
TiO2	0,34	0,33	0,00	0,00	0,29	0,52	0,30	0,29	0,00	0,00	0,39	0,00
Al2O3	27,87	28,20	28,57	27,38	25,58	27,49	27,62	29,35	34,37	33,92	33,30	38,74
FeO	2,94	2,99	2,75	4,93	2,50	3,45	2,00	2,59	1,26	2,50	1,38	0,80
MgO	2,60	2,60	2,57	3,44	3,17	2,77	3,41	2,57	1,17	1,46	1,28	0,48
CaO	0,00	0,00	0,00	0,00	0,00	0,00	0,00	0,00	0,00	0,00	0,00	0,00
Na2O	0,43	0,40	0,45	0,00	0,00	0,00	0,38	0,52	1,36	2,95	0,76	6,90
K2O	9,50	9,63	9,71	10,21	9,47	10,21	8,75	8,67	8,01	5,74	8,52	0,64
	******	******	******	******	******	******	******	******	******	******	******	******
Total	95,00	95,00	95,00	95,00	95,00	95,00	95,00	95,00	95,00	95,00	95,00	95,00
Si	6,833	6,781	6,787	6,650	7,134	6,780	6,918	6,745	6,407	6,356	6,487	6,074
Al IV	1,167	1,219	1,213	1,350	0,866	1,220	1,082	1,255	1,593	1,644	1,513	1,926
Al VI	3,206	3,214	3,271	3,025	3,118	3,126	3,205	3,319	3,724	3,603	3,644	3,918
Ti	0,034	0,033	0,000	0,000	0,028	0,053	0,030	0,028	0,000	0,000	0,038	0,000
Fe	0,327	0,334	0,306	0,559	0,276	0,387	0,221	0,287	0,139	0,274	0,151	0,085
Mg	0,517	0,518	0,511	0,695	0,625	0,555	0,670	0,508	0,229	0,286	0,251	0,092
Ca	0,000	0,000	0,000	0,000	0,000	0,000	0,000	0,000	0,000	0,000	0,000	0,000
Na	0,110	0,103	0,115	0,000	0,000	0,000	0,097	0,134	0,346	0,752	0,194	1,712
K	1,614	1,639	1,650	1,767	1,597	1,747	1,470	1,463	1,341	0,961	1,428	0,104
Z	8,000	8,000	8,000	8,000	8,000	8,000	8,000	8,000	8,000	8,000	8,000	8,000
Y	4,084	4,098	4,088	4,279	4,047	4,120	4,125	4,141	4,091	4,164	4,085	4,096
X	1,724	1,742	1,765	1,767	1,597	1,747	1,567	1,597	1,687	1,713	1,622	1,816
Xmg	0,613	0,608	0,626	0,554	0,694	0,589	0,752	0,639	0,622	0,511	0,624	0,520
Ms	0,936	0,941	0,935	1,000	1,000	1,000	0,938	0,916	0,795	0,561	0,881	0,057
Pg	0,064	0,059	0,065	0,000	0,000	0,000	0,062	0,084	0,205	0,439	0,119	0,943
Mrg	0,000	0,000	0,000	0,000	0,000	0,000	0,000	0,000	0,000	0,000	0,000	0,000

Dioctahedral micas

SAMPLE	*ADY10*								ADY17			
SiO2	52,46	52,41	52,07	49,92	47,07	47,19	48,07	47,25	50,32	49,94	51,96	50,09
TiO2	0,00	0,00	0,00	0,00	0,00	0,00	0,00	0,00	0,00	0,39	0,34	0,00
Al2O3	26,10	26,29	26,35	25,17	35,99	35,89	34,91	34,09	26,81	31,40	28,80	33,15
FeO	2,31	2,14	2,35	6,03	1,24	1,05	1,10	2,38	5,05	1,78	1,94	0,90
MgO	3,81	3,81	3,78	3,14	0,67	0,58	0,78	1,59	2,70	2,18	2,94	0,00
CaO	0,00	0,00	0,00	0,82	0,00	0,00	0,00	0,00	0,00	0,00	0,00	1,47
Na2O	0,29	0,29	0,32	0,00	1,03	0,98	1,08	0,76	0,37	0,53	0,29	2,38
K2O	10,02	10,07	10,13	9,92	9,01	9,31	9,06	8,94	9,75	8,79	8,73	7,00
	******	******	******	******	******	******	******	******	******	******	******	******
Total	95,00	95,00	95,00	95,00	95,00	95,00	95,00	95,00	95,00	95,00	95,00	95,00
Si	6,980	6,968	6,938	6,810	6,218	6,237	6,341	6,279	6,798	6,586	6,837	6,563
Al IV	1,020	1,032	1,062	1,190	1,782	1,763	1,659	1,721	1,202	1,414	1,163	1,437
Al VI	3,073	3,088	3,077	2,856	3,821	3,827	3,769	3,618	3,066	3,466	3,303	3,683
Ti	0,000	0,000	0,000	0,000	0,000	0,000	0,000	0,000	0,000	0,039	0,034	0,000
Fe	0,257	0,238	0,261	0,688	0,136	0,117	0,122	0,264	0,571	0,196	0,213	0,099
Mg	0,755	0,755	0,751	0,639	0,133	0,114	0,153	0,314	0,543	0,428	0,576	0,000
Ca	0,000	0,000	0,000	0,119	0,000	0,000	0,000	0,000	0,000	0,000	0,000	0,207
Na	0,076	0,073	0,083	0,000	0,263	0,251	0,277	0,196	0,097	0,136	0,075	0,606
K	1,701	1,708	1,722	1,726	1,518	1,570	1,525	1,515	1,680	1,478	1,466	1,170
Z	8,000	8,000	8,000	8,000	8,000	8,000	8,000	8,000	8,000	8,000	8,000	8,000
Y	4,085	4,081	4,090	4,184	4,090	4,058	4,044	4,196	4,180	4,128	4,126	3,782
X	1,777	1,782	1,805	1,845	1,781	1,820	1,802	1,711	1,777	1,614	1,541	1,983
Xmg	0,746	0,761	0,742	0,482	0,493	0,495	0,558	0,544	0,488	0,686	0,730	0,000
Ms	0,957	0,959	0,954	0,935	0,852	0,862	0,846	0,886	0,945	0,916	0,951	0,590
Pg	0,043	0,041	0,046	0,000	0,148	0,138	0,154	0,114	0,055	0,084	0,049	0,306
Mrg	0,000	0,000	0,000	0,065	0,000	0,000	0,000	0,000	0,000	0,000	0,000	0,104

Table S4: Representative microprobe analyses of dioctahedral micas of Châtel Argent Castle (ACK04, ACK10, ACK12) and Quart Castle (ADY04, ADY10). The chemical composition of minerals is expressed as weight% oxides. The structural formulae, reported as number of cations per formula unit (a.p.f.u.), were recalculated on the basis of 22 oxygens. X= Interlayer site, Z= Tetrahedral site, Y= Octahedral site, Xmg= Mg/(Mg+Fe^{2+}+Fe^{3+}). Ms= Muscovite, Pg= Paragonite, Mrg= Margarite (Mineral abbreviations according to Whitney and Evans, 2010).

Triocthedral micas

SAMPLE	*ADY04*	*ADY10*		*ADY17*		
SiO2	39,80	36,25	36,06	36,05	37,03	36,75
TiO2	1,76	4,44	4,40	4,39	4,98	4,83
Al2O3	15,84	17,44	17,54	17,31	17,63	17,31
FeO	15,70	18,60	19,10	19,55	16,08	15,96
MgO	14,72	10,25	10,40	9,65	11,21	12,34
Na2O	0,00	0,00	0,00	0,00	0,00	0,00
K2O	8,19	9,02	8,51	9,06	9,06	8,82
	******	******	******	******	******	******
Total	96,00	96,00	96,00	96,00	96,00	96,00
Si	5,817	5,440	5,410	5,439	5,480	5,436
Al IV	2,183	2,560	2,590	2,561	2,520	2,564
Al VI	0,545	0,525	0,511	0,517	0,555	0,454
Ti	0,193	0,501	0,496	0,498	0,555	0,537
Fe	1,918	2,334	2,397	2,466	1,990	1,974
Mg	3,206	2,294	2,325	2,170	2,473	2,720
Ca	0,000	0,000	0,000	0,000	0,000	0,000
Na	0,000	0,000	0,000	0,000	0,000	0,000
K	1,527	1,728	1,628	1,744	1,711	1,665
Z	8,000	8,000	8,000	8,000	8,000	8,000
Y	5,863	5,653	5,729	5,652	5,573	5,685
X	1,527	1,728	1,628	1,744	1,711	1,665
Xmg	0,626	0,496	0,492	0,468	0,554	0,580

Table S5: Representative microprobe analyses of trioctahedral micas of Quart Castle (ADY04, ADY10 and ADY17). The chemical composition of minerals is expressed as weight% oxides. The structural formulae, reported as number of cations per formula unit (a.p.f.u.), were recalculated on the basis of 22 oxygens. X= Interlayer site, Z= Tetrahedral site, Y= Octahedral site, Xmg= Mg/(Mg+Fe^{2+}+Fe^{3+}).

Petrographic characterization of historic mortar as a tool in archeologic study: examples from two medieval castles of Aosta Valley, Northwestern Italy

E. Milanesio[1], E. Storta[1*], F. Gambino[1], L. Appolonia[2], A. Borghi[1], A. Glarey[2]

1 Department of Earth Sciences, University of Turin, Via Valperga Caluso 35, Torino 10125, Italy

2 Dipartimento soprintendenza per i beni e le attività culturali, Assessorato istruzione e cultura, Regione Autonoma Valle d'Aosta, Piazza Narbonne, n.3-11100 Aosta, Italy

*Corresponding Author: E-mail address: elena.storta@unito.it (Elena Storta)

Consent for publication

All authors gave consent for publication on the Resources Policy

Authors' contributions

Field work: EM, ES; conceptualization: EM, ES, AB, FG, LA, AB and AG; data collection: EM, ES and LA; data analysis: EM, ES, FG, LA, AB and AG; archaeological framework: EM, LA and AG; writing original draft: EM and ES; figures draft and editing: EM and ES; validation: EM, ES, FG, LA, AB and AG; writing, review and editing: EM, ES, FG, LA, AB and AG. All authors read and approved the final manuscript.

Competing interests

The authors declare that they have no competing interests.

Declaration of Competing Interest

The authors declare that they have no known competing financial interests or personal relationships that could have appeared to influence the work reported in this paper.